Infrared Spectroscopy of Carboions. 8. Hollow Cathode Spectroscopy of Protonated Acetylene, C2H3+

ARTICLE *in* THE JOURNAL OF PHYSICAL CHEMISTRY · OCTOBER 1995

Impact Factor: 2.78 · DOI: 10.1021/j100042a042

5 AUTHORS, INCLUDING:

Dairene Uy
Ford Motor Company
48 PUBLICATIONS **651** CITATIONS
SEE PROFILE

Takeshi Oka
University of Chicago
337 PUBLICATIONS **8,591** CITATIONS
SEE PROFILE

Takayoshi Amano
University of Waterloo
170 PUBLICATIONS **2,943** CITATIONS
SEE PROFILE

Infrared Spectroscopy of Carboions. 8. Hollow Cathode Spectroscopy of Protonated Acetylene, $C_2H_3^+$

C. M. Gabrys, D. Uy, M.-F. Jagod, and T. Oka*

Department of Chemistry and Department of Astronomy and Astrophysics, The University of Chicago, Chicago, Illinois 60637-1403

T. Amano

Institute for Astrophysics and Planetary Sciences, Ibaraki University, Mito, Ibaraki, Japan

Received: June 21, 1995[⊗]

The vibration−rotation energy level pattern of protonated acetylene, $C_2H_3^+$, in the ν_6 (C−H antisymmetric stretching) vibrational state is anomalous and irregular because of the coupling between the rotational motion and the tunneling of the three protons among their equilibrium positions. The resultant spectral anomaly and the coexistence of C−H bands of other carbocations such as CH_3^+, $C_2H_2^+$, CH_2^+, etc., in our positive column discharge using He-dominated gas mixtures had made the analysis of the $C_2H_3^+$ spectrum difficult. In the present paper we use a hollow cathode discharge to simplify plasma chemistry and to make a more definitive and extensive analysis of the spectrum. A 3 m hollow cathode discharge cell has been constructed with a multiple reflection optical system giving an effective path length of 30 m. A gas mixture of C_2H_2 and H_2 with pressures of 0.03 and 1.1 Torr, respectively, has produced spectral lines of $C_2H_3^+$ from 3192 to 3083 cm^{-1} which are almost completely free of those from other carbocations. The purity of the spectrum, together with the accurate ground state rotational constants recently reported by the Lille millimeter wave group, has allowed us to assign spectral lines up to $J = 25$ and $K_a = 4$ and to determine extensive sets of the A−E splittings due to the proton tunneling in the excited state. An attempt has been made to analyze the plasma chemistry in the hollow cathode on the basis of earlier plasma diagnostic studies of the negative glow region. A model was used in which the primary molecular ions H_2^+ and $C_2H_2^+$ are generated due to ionization by "hot" primary and secondary electrons. In the plasma these ions undergo ion−neutral reactions to produce H_3^+ and $C_2H_3^+$, which are dissociated by reactions with C_2H_2 and recombination with "ultimate" electrons. By assuming proper number densities of primary, secondary, and ultimate electrons, semiquantitative agreement with the experimentally estimated ion densities has been obtained.

1. Introduction

Positive column discharges of helium-dominated gas mixtures, containing small amounts of hydrocarbon and hydrogen in varying concentration ratios, produce many simple carbocations whose infrared vibration−rotation spectra may be detected through their CH stretching vibrations in the 3.2 μm region.[1] Using our difference-frequency laser system as the tunable infrared radiation source[2] and the velocity modulation technique as the detection method,[3] we have observed over 5000 ion spectral lines in the wavenumber region between 3300 and 2900 cm^{-1}. In this thicket of spectral lines we have so far identified spectra of four carbocations, CH_2^+,[4] CH_3^+,[5−7] $C_2H_2^+$,[8,9] and $C_2H_3^+$.[10] Approximately 15% of the observed ion spectral lines have been assigned to either these species or H_3^+ and HeH^+ and impurity ions such as HCO^+, HN_2^+, and $HCNH^+$. Spectra of isotopic species $^{13}CH_3^+$,[6] $^{13}C_2H_2^+$,[9] $HCCD^+$,[9,11] CH_2D^+,[11,12] and CHD_2^+[12] have also been identified in isotopically enriched plasmas.

The assignment of the complicated spectral pattern of these carbocations, which had not previously been studied in any spectral region, proceeds in the following steps. First, velocity modulation allows us to observe only ion signals; without this technique it would be very hard to study carbocations since the stable neutral molecules and even free radicals produced in plasmas have concentrations several orders of magnitude higher than those of ions, and their spectra would dominate the CH stretching region. Second, the Doppler-broadened spectral linewidths, which are inversely proportional to the square root of the moving particles' masses, allow us to discriminate spectral lines due to hydrocarbon cations containing one carbon atom from those containing two or more carbon atoms. Third, a variation of plasma chemical conditions such as pressure, temperature, electric current, and the mixing ratios of constituent gases often allows us to identify groups of spectral lines belonging to specific carriers. Finally, a recognition of the theoretical spectral pattern in the observed spectral lines allows us to identify the carrier of the lines and to assign the individual transitions. This last step is trivial if the ion is an ordinary linear molecule and is relatively straightforward if it is a "well-behaving" symmetric or asymmetric top molecule. Thus, for example, the identification of the spectra of CH_3^+ and $C_2H_2^+$ and their deuterated species was relatively simple. A characteristic difficulty of carbocation spectroscopy, however, is that the spectral pattern is often anomalous. There are a variety of reasons for the anomaly. The spectrum of $C_2H_3^+$ is anomalous because the three protons tunnel among their equilibrium positions,[10] as discussed further below. A similar but more drastic complication is expected[13] for CH_5^+. The spectrum of CH_2^+ is anomalous because of the Renner−Teller interaction and the low barrier to linearity in the ground electronic state.[4] To sort out spectral lines with such anomalous patterns, it is necessary to rely more on chemical discrimination.

* Author to whom correspondence should be addressed.
⊗ Abstract published in *Advance ACS Abstracts,* October 1, 1995.

0022-3654/95/2099-15611$09.00/0

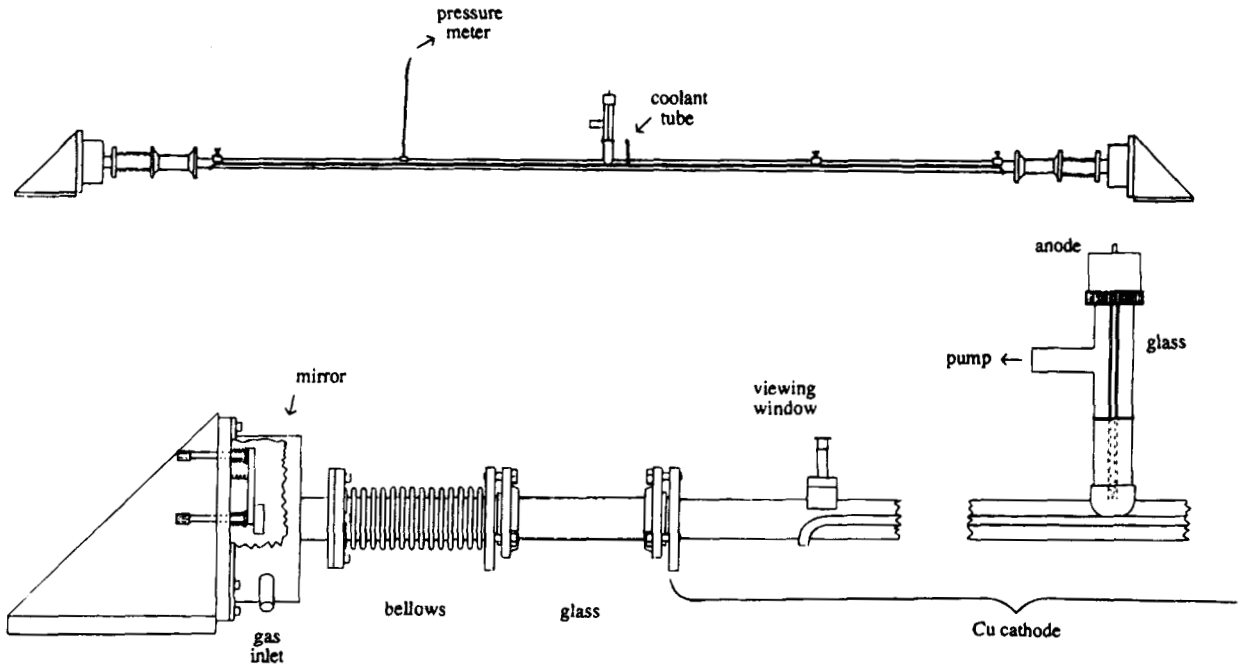

Figure 1. Diagrams of the hollow cathode. The design is similar to the hollow cathode constructed earlier by C. J. Pursell for infrared−microwave double-resonance experiments on molecular ions. A peak discharge current of 1.75 A was drawn through the cell, and the plasma extended ≥1.5 m at the central region of the tubular cathode. See text for details.

This paper marks the inception of our use of hollow cathode discharges for carboion spectroscopy. Unlike the positive column discharges we have used so far, in which the plasma is contained in a Pyrex glass tube, the plasma in a hollow cathode is contained in a metal tube. The discharge is sustained by photoelectric ejection of electrons from the metal, resulting in

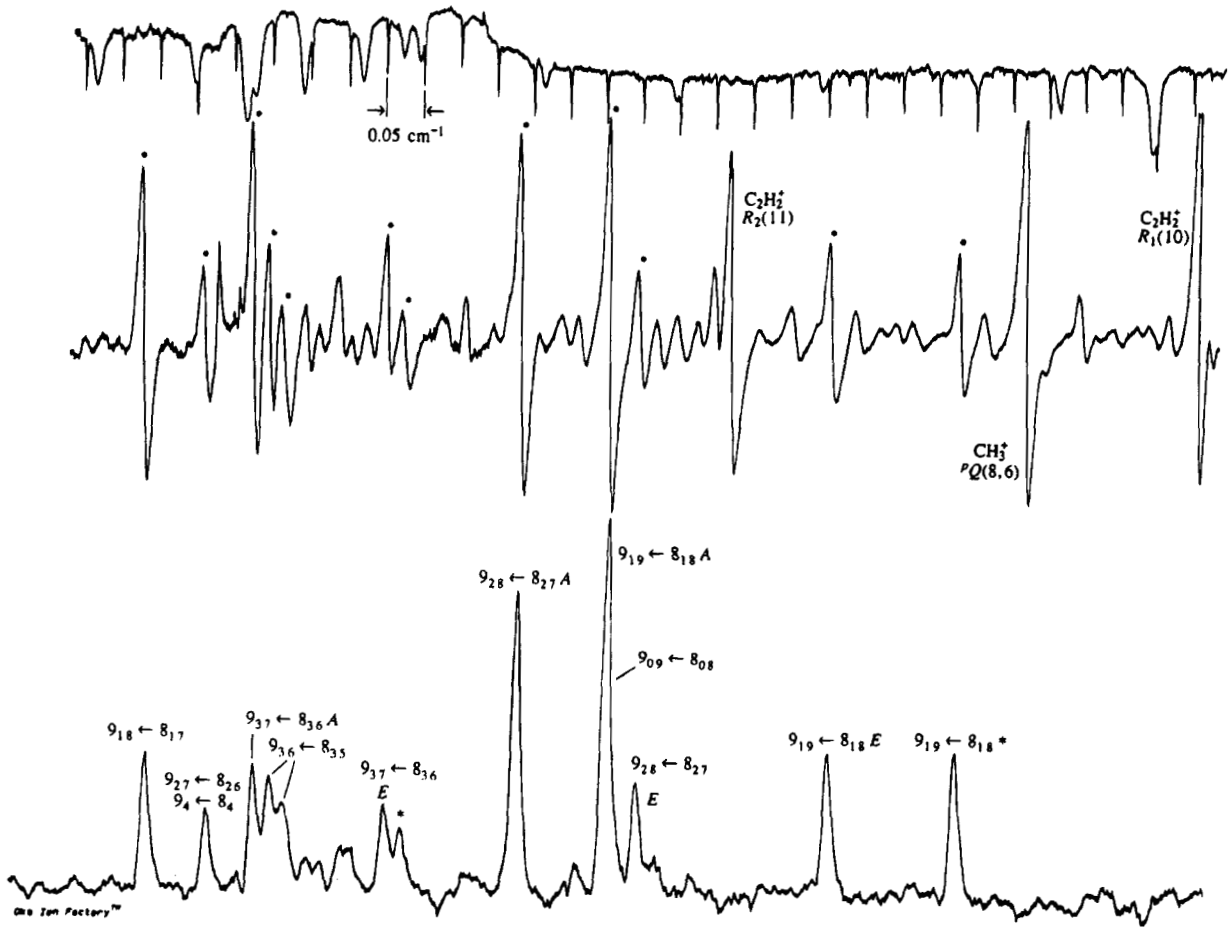

Figure 2. Comparison of a spectrum recorded by using a positive column discharge with a He-dominated gas mixture $He/H_2/CH_4$ = 7/0.1/0.12 Torr (upper trace) and one recorded by using the hollow cathode discharge with a gas mixture H_2/C_2H_2 = 1.1/0.03 Torr (lower trace). The spectral region for the R(8) transitions of $C_2H_3^+$ from 3161.75 to 3160.23 cm^{-1} is shown. The uppermost trace shows C_2H_4 lines and wavenumber markers (separated by 0.05 cm^{-1}) for measurements. Note that CH_3^+ and $C_2H_2^+$ lines are absent in the hollow cathode spectrum.

a high concentration of low-temperature electrons. Naturally, the plasma chemistry in a hollow cathode is very different from that in a positive column. Over the years, Amano[14] has been very successful in developing hollow cathode spectroscopy and discovered spectra of many protonated ions such as $HOCO^+$,[15] $NNOH^+$,[16] SH_3^+,[17] $HOCS^+$,[18] HC_3NH^+,[19] CH_3CNH^+,[20] H_2COH^+,[21] and $HNCCN^+$.[22] Indeed our earlier work on the anomalous $C_2H_3^+$ spectrum[10] was helped by a hollow cathode spectrum provided by Amano, which showed some low-J regions of the spectrum entirely free of lines due to any other molecule. Thus, we anticipated being able to selectively observe spectra of protonated carbocations such as protonated acetylene, $C_2H_3^+$, and protonated methane, CH_5^+. In this paper we report our extension of the $C_2H_3^+$ spectroscopy using a hollow cathode discharge.

Protonated acetylene, $C_2H_3^+$, is especially interesting because of the possible existence of two conformers, the classical and the nonclassical structure, that are nearly equal in energy. Since the literature on $C_2H_3^+$ prior to 1989 was extensively quoted in our previous paper,[10] we here quote only works after 1989. In that paper[10] we concluded experimentally that (1) the H-bridged nonclassical structure is lower in energy than the classical structure and (2) the apex proton and the two end protons exchange their positions sufficiently rapidly that the effect is observed as a splitting of spectral lines in the excited vibrational state. Using a simple internal rotation model with a 6-fold barrier, the barrier height was estimated to be $V_6 \geq 6.0$ kcal/mol, and this was also interpreted to be the energy difference between the two structures. This value was challenged by three theoretical groups; Liang, Hamilton, and Schaefer[23] gave 4.0 kcal/mol, Klopper and Kutzelnigg[24] gave 4.5 kcal/mol, and Lindh, Rice, and Lee[25] gave 3.7 ± 1.3 kcal/mol. Since the internal rotation model with a 6-fold barrier is very crude and tends to give a larger barrier, our value was perhaps overestimated.

A major experimental advance occurred recently when the Lille millimeter wave group observed[26] an extensive rotational spectrum of $C_2H_3^+$. Their result not only confirmed the infrared results[10] and improved the accuracy of the B and C rotational constants but also provided the A rotational constant, which agreed well with the prediction by *ab initio* calculation and thus provided further evidence for the nonclassical structure of $C_2H_3^+$. The observed inertial defect of 0.0848 amu Å^2 is approximately the magnitude expected for this type of molecule due to zero-point vibration,[27] and it established the planarity of $C_2H_3^+$. Their results have also provided radio astronomers with accurate spectral frequencies of $C_2H_3^+$, which is expected to be abundant in interstellar molecular clouds.[28] More recently, they have observed evidence of spectral splitting in the ground vibrational state due to the proton-tunneling motion,[29] whose order of magnitude agrees well with the prediction by Escribano, Bunker, and Gomez.[30] From the analysis of the observed splittings, the barrier height has been estimated to be 1642 cm^{-1} (4.7 kcal/mol), which is slightly higher than the predicted *ab initio* values.[23-25]

A puzzling analysis of experimental results obtained by the Coulomb explosion imaging (CEI) method has been reported by Vager *et al.*[31] recently. In this paper they note that "the nuclear conformations in the molecule ($C_2H_3^+$) differ markedly from theoretical predictions and previous experimental findings". They propose a new nonplanar configuration in which a proton is revolving around a *trans*-bent acetylene frame. As for the discrepancy with their own previous result,[32] they note that "the use of the assumption of a localized conformation in the previous CEI analysis led to a bridged structure, the same *erroneous* result found in the spectroscopic studies" (our italics). This new structure of $C_2H_3^+$ is incompatible with the infrared[10] and millimeter wave[26] spectroscopic results, which we believe are definitive.

In view of the special interest of protonated acetylene, we have conducted extensive hollow cathode spectroscopy. The object of this work is 3-fold: (a) to confirm earlier identification and to provide more extensive experimental information on the proton-tunneling splitting in the excited vibrational state, (b) to discriminate $C_2H_3^+$ spectral lines from those of other unknown species to help in the identification of the latter, and (c) to study the properties of hollow cathode plasmas, pointing toward their application to the spectroscopy of other protonated ions, in particular CH_5^+.

2. Experimental Section

The experiment was performed with our existing difference-frequency infrared source and a newly constructed copper hollow cathode cell. In the difference-frequency source, developed by Pine,[2,33] the outputs from two visible lasers, one a fixed-frequency single-mode argon ion laser and the other a tunable dye laser operating with R6G, are collinearly passed through a 5 cm long $LiNbO_3$ crystal, which converts about 10^{-4} of the incoming power to infrared at the difference of the visible frequencies. The spectral purity of the infrared radiation is about 10 MHz. About half of the infrared radiation was passed 20 times through the plasma in a hollow cathode by reflection off White cell mirrors enclosed in the space evacuated for the discharge, and the absorption signal was detected with an InSb photovoltaic diode. The other half of the radiation was sent straight to a matched detector for source amplitude noise subtraction. A small portion was sent through a sample of C_2H_4 for wavenumber calibration.

The hollow cathode is shown in Figure 1. Unlike Amano's hollow cathode, which is enclosed in an evacuated glass container, the hollow cathode itself forms a vacuum chamber. This design was introduced into our group by C. J. Pursell and used for infrared−microwave double-resonance experiments in plasmas.[34-36] The tubular cathode has a 1−3/8 in. inner diameter and is 3 m long to allow the plasma inside to extend as far as possible and to fit tightly around the beam volume defined by the diameter of the White cell mirrors. The extent of the plasma is monitored through viewing windows; the most we could achieve was a length along the path of ≳1.5 m, providing a 30 m path length after 20 traversals. Since the White cell mirrors have a radius of curvature, equal to their separation, of 3.8 m, the cathode is joined on either side to 6 in. long glass tubes to protect the mirrors from a fully extended discharge (which was never a problem), and the glass is followed by 6 in. lengths of bellows to isolate the White cell mirror mounts from vibration of the pump. The anode is a 1/4 in. diameter stainless steel rod, pointed at the end, which hangs at the center. This symmetric construction is similar to that used originally by Van den Heuvel and Dymanus.[37] A gas mixture is fed into the cathode from ports near the mirrors on both ends and is pumped out at the anode with a 10 L/s mechanical pump preceded by a liquid-N_2 trap. A mixture of 30 mTorr C_2H_2 and 1.1 Torr H_2 was found to optimize the $C_2H_3^+$ signals.

The ac discharge is powered at 11 kHz by an ENI RS-16B synthesizer-amplifier. The current is conducted through the plasma only during the half-cycle when the anode is positively charged; that is, the anode−hollow cathode system acts as a rectifier, providing a means for ion concentration modulation.[38] Actually in a cathode of our diameter filled with gas at the pressure we intended to use, this rectification breaks down at a

TABLE 1: Observed Spectral Lines of $C_2H_3^+$ and the Ground State Combination Differences (in cm^{-1})[i]

R			P			C.D.		δ
$1_{01} \leftarrow 0_{00}$ #		3144.758	$1_{01} \leftarrow 2_{02}$ #		3138.190[§]	$2_{02} - 0_{00}$	6.568	0.003
$2_{02} \leftarrow 1_{01}$	A	3146.626	$2_{02} \leftarrow 3_{03}$	A	3135.684	$3_{03} - 1_{01}$	10.941	0.002
	E	3146.286		E	3135.346		10.940	0.000
$2_{11} \leftarrow 1_{10}$	A	3146.713	$2_{11} \leftarrow 3_{12}$	A	3135.536	$3_{12} - 1_{10}$	11.177	−0.002
	E	3146.508		E	3135.326		11.182	0.004
$2_{12} \leftarrow 1_{11}$		3146.360	$2_{12} \leftarrow 3_{13}$		3135.659	$3_{13} - 1_{11}$	10.701	0.000
			$2_2 \leftarrow 3_2$		3135.395			
$3_{03} \leftarrow 2_{02}$ #		3148.352	$3_{03} \leftarrow 4_{04}$		3133.041	$4_{04} - 2_{02}$	15.311	0.000
$3_{12} \leftarrow 2_{11}$		*3149.137	$3_{12} \leftarrow 4_{13}$		*3133.479	$4_{13} - 2_{11}$	15.658	0.009
		*3148.950			*3133.299		15.651	0.002
$3_{13} \leftarrow 2_{12}$	A	3148.439	$3_{13} \leftarrow 4_{14}$	A	3133.458	$4_{14} - 2_{12}$	14.981	0.001
	E	3148.850		E	3133.869		14.981	0.001
		*3148.816			*3133.830		14.985	0.005
$3_{21} \leftarrow 2_{20}$		3148.211	$3_{21} \leftarrow 4_{22}$		3132.894	$4_{22} - 2_{20}$	15.317	0.002
$3_{22} \leftarrow 2_{21}$ #		3147.684	$3_{22} \leftarrow 4_{23}$		3132.379	$4_{23} - 2_{21}$	15.305	−0.003
			$3_3 \leftarrow 4_3$		3133.286			
$4_{04} \leftarrow 3_{03}$	A	3150.912	$4_{04} \leftarrow 5_{05}$	A	3131.234	$5_{05} - 3_{03}$	19.678	−0.001
	E	3150.839[§]		E	3131.167		19.672	−0.006
$4_{13} \leftarrow 3_{12}$	A	3150.896	$4_{13} \leftarrow 5_{14}$	A	3130.777	$5_{14} - 3_{12}$	20.119	0.001
	E	3150.839[§]		E	3130.723		20.116	−0.003
$4_{14} \leftarrow 3_{13}$		3150.552[§]	$4_{14} \leftarrow 5_{15}$		3131.295	$5_{15} - 3_{13}$	19.258	−0.001
$4_{22} \leftarrow 3_{21}$	A	3150.839[§]	$4_{22} \leftarrow 5_{23}$	A	3131.140	$5_{23} - 3_{21}$	19.699	0.003
	E	3150.552[§]		E	3130.859		19.693	−0.003
		*3150.253			*3130.555		19.697	0.001
$4_{23} \leftarrow 3_{22}$		3150.310	$4_{23} \leftarrow 5_{24}$		3130.630	$5_{24} - 3_{22}$	19.679	0.000
$4_3 \leftarrow 3_3$ #		3150.736	$4_3 \leftarrow 5_3$		3131.072	$5_{32} - 3_{30}$	19.664	−0.002
		3150.703			3131.041		19.662	−0.004
$5_{05} \leftarrow 4_{04}$		3152.904[§]	$5_{05} \leftarrow 6_{06}$		3128.865	$6_{06} - 4_{04}$	24.039	−0.002
$5_{14} \leftarrow 4_{13}$		3152.994	$5_{14} \leftarrow 6_{15}$		3128.407	$6_{15} - 4_{13}$	24.586	0.001
$5_{15} \leftarrow 4_{14}$	A	3152.639	$5_{15} \leftarrow 6_{16}$	A	3129.104[§]	$6_{16} - 4_{14}$	23.535	0.001
	E	3152.678[§]		*E*	3129.140		23.538	0.003
$5_{23} \leftarrow 4_{22}$		3152.904[§]	$5_{23} \leftarrow 6_{24}$		3128.826	$6_{24} - 4_{22}$	24.078	−0.003
$5_{24} \leftarrow 4_{23}$	A	3152.682[§]	$5_{24} \leftarrow 6_{25}$	A	3128.633	$6_{25} - 4_{23}$	24.049	−0.001
	E	3152.313		E	3128.261		24.051	0.001
$5_3 \leftarrow 4_3$	A	3152.837	$5_3 \leftarrow 6_3$	A	3128.803	$6_3 - 4_3$	24.033	−0.004
	E	3153.061		E	3129.024		24.037	0.001
$5_4 \leftarrow 4_4$		3153.100	$5_4 \leftarrow 6_4$		3129.104[§]	$6_4 - 4_4$	23.996	−0.008
		3153.171			3129.170		24.001	−0.003
$6_{06} \leftarrow 5_{05}$ #	A	3154.757	$6_{06} \leftarrow 7_{07}$ #	A	3126.360	$7_{07} - 5_{05}$	28.397	0.000
	E	3154.861[§]		E	3126.468[§]		28.393	−0.004
$6_{15} \leftarrow 5_{14}$	A	3155.203[§]	$6_{15} \leftarrow 7_{16}$	A	3126.149	$7_{16} - 5_{14}$	29.054	0.002
	E	3155.263		E	3126.210		29.053	0.002
$6_{16} \leftarrow 5_{15}$		3154.670	$6_{16} \leftarrow 7_{17}$		3126.860	$7_{17} - 5_{15}$	27.810	0.000
$6_{24} \leftarrow 5_{23}$ #	A	3154.483[a]	$6_{24} \leftarrow 7_{25}$ #	A	3126.015	$7_{25} - 5_{23}$	28.468	−0.003
	E	3154.796		E	3126.326		28.471	0.000
$6_{25} \leftarrow 5_{24}$ #		3154.936[§]	$6_{25} \leftarrow 7_{26}$ #		3126.516[§]	$7_{26} - 5_{24}$	28.421	0.001
$6_3 \leftarrow 5_3$	A	3154.868[§]	$6_3 \leftarrow 7_3$		3126.468[b§]	$7_3 - 5_3$	28.400	−0.008
		3154.861[§]			3126.468[b§]		28.393	−0.015
	E	3154.811			3126.408		28.403	−0.005
$6_4 \leftarrow 5_4$		3155.106	$6_4 \leftarrow 7_4$		3126.741	$7_4 - 5_4$	28.365	−0.003
		3155.203[§]			3126.836		28.367	−0.001
$6_5 \leftarrow 5_5$		3155.187	$6_5 \leftarrow 7_5$		3126.875	$7_5 - 5_5$	28.313	−0.007
$7_{07} \leftarrow 6_{06}$		3157.317	$7_{07} \leftarrow 8_{08}$ #		3124.569	$8_{08} - 6_{06}$	32.748	0.003
$7_{16} \leftarrow 6_{15}$		3157.397[§]	$7_{16} \leftarrow 8_{17}$		3123.880	$8_{17} - 6_{15}$	33.516	0.002
$7_{17} \leftarrow 6_{16}$	A	3156.961	$7_{17} \leftarrow 8_{18}$	A	3124.878	$8_{18} - 6_{16}$	32.082	0.000
	E	3156.863		E	3124.778		32.085	0.002
$7_{25} \leftarrow 6_{24}$		*3157.397[§]	$7_{25} \leftarrow 8_{26}$		*3124.533[§]	$8_{26} - 6_{24}$	32.863	−0.003
		*3157.101			*3124.238		32.863	−0.003
$7_{26} \leftarrow 6_{25}$	A	3156.928	$7_{26} \leftarrow 8_{27}$	A	3124.138	$8_{27} - 6_{25}$	32.790	0.003
	E	3156.878		E	3124.091		32.787	−0.001
$7_3 \leftarrow 6_3$		3157.418	$7_3 \leftarrow 8_3$		3124.638	$8_3 - 6_3$	32.780	0.000
		3157.069			3124.282		32.787	0.008
$7_4 \leftarrow 6_4$		3157.295	$7_4 \leftarrow 8_4$		3124.554	$8_4 - 6_4$	32.742	0.009
		3157.273			3124.533[§]		32.740	0.007
$7_5 \leftarrow 6_5$		3157.368	$7_5 \leftarrow 8_5$		3124.698	$8_5 - 6_5$	32.671	−0.006
$8_{08} \leftarrow 7_{07}$ #	A	3158.885	$8_{08} \leftarrow 9_{09}$ #	A	3121.801	$9_{09} - 7_{07}$	37.084	−0.001
	E	3158.854		E	3121.774		37.080	−0.005
$8_{17} \leftarrow 7_{16}$	A	3159.510	$8_{17} \leftarrow 9_{18}$	A	3121.535	$9_{18} - 7_{16}$	37.975	0.000
	E	3159.490		E	3121.516		37.974	−0.001
$8_{18} \leftarrow 7_{17}$		3158.854	$8_{18} \leftarrow 9_{19}$		3122.500	$9_{19} - 7_{17}$	36.354	0.002
$8_{26} \leftarrow 7_{25}$ #	A	3159.040	$8_{26} \leftarrow 9_{27}$	A	3121.774	$9_{27} - 7_{25}$	37.266	−0.002
	E	3159.188[§]		E	3121.923[§]		37.266	−0.001
		*3159.248			*3121.982		37.266	−0.001
$8_{27} \leftarrow 7_{26}$		3159.076	$8_{27} \leftarrow 9_{28}$		3121.923[§]	$9_{28} - 7_{26}$	37.153	−0.001

TABLE 1 (Continued)

R			P			C.D.		δ
$8_3 \leftarrow 7_3$		3159.312	$8_3 \leftarrow 9_3$		3122.166[b]	$9_3 - 7_3$	37.147	−0.006
		3159.318					37.152	0.000
		3159.228			3122.076[§]		37.152	−0.001
$8_4 \leftarrow 7_4$		3159.445	$8_4 \leftarrow 9_4$		3122.360	$9_4 - 7_4$	37.086	−0.012
		3159.169			3122.076[§]		37.093	−0.005
		3159.188[§]			3122.103		37.085	−0.013
$9_{09} \leftarrow 8_{08}$ #		3161.044[§]	$9_{09} \leftarrow 10_{0,10}$ #		3119.629	$10_{0,10} - 8_{08}$	41.414	0.000
$9_{18} \leftarrow 8_{17}$ #		3161.663	$9_{18} \leftarrow 10_{19}$		3119.231	$10_{19} - 8_{17}$	42.432	0.000
$9_{19} \leftarrow 8_{18}$	A	3161.044[§]	$9_{19} \leftarrow 10_{1,10}$	A	3120.424	$10_{1,10} - 8_{18}$	40.620	0.000
	E	3160.744		E	3120.123[§]		40.621	0.001
		*3160.570			*3119.947[§]		40.623	0.003
$9_{27} \leftarrow 8_{26}$		3161.581[§]	$9_{27} \leftarrow 10_{28}$		3119.892	$10_{28} - 8_{26}$	41.689	0.013
$9_{28} \leftarrow 8_{27}$	A	3161.163	$9_{28} \leftarrow 10_{29}$	A	3119.645	$10_{29} - 8_{27}$	41.518	0.000
	E	3161.002		E	3119.483		41.519	0.001
$9_{36} \leftarrow 8_{35}$		3161.496	$9_{36} \leftarrow 10_{37}$		3119.966	$10_{37} - 8_{35}$	41.530	0.003
		3161.477			3119.947[§]		41.530	0.003
$9_{37} \leftarrow 8_{36}$	A	3161.518	$9_{37} \leftarrow 10_{38}$	A	3119.993	$10_{38} - 8_{36}$	41.525	0.000
	E	3161.341		E	3119.817		41.524	−0.001
		*3161.319			*3119.793		41.525	0.001
$9_4 \leftarrow 8_4$		3161.581[§]	$9_4 \leftarrow 10_4$		3120.123[§]	$10_4 - 8_4$	41.458	−0.005
$10_{0,10} \leftarrow 9_{09}$	A	3163.379	$10_{0,10} \leftarrow 11_{0,11}$ #	A	3117.646	$11_{0,11} - 9_{09}$	45.733	0.000
	E	3163.356		E	3117.623		45.733	0.000
		*3163.824			*3118.094		45.731	−0.003
$10_{19} \leftarrow 9_{18}$	A	3163.759	$10_{19} \leftarrow 11_{1,10}$	A	3116.874	$11_{1,10} - 9_{18}$	46.885	−0.001
	E	3163.702		E	3116.819		46.883	−0.003
		*3162.992[§]			*3116.110		46.882	−0.004
$10_{1,10} \leftarrow 9_{19}$		3162.856	$10_{1,10} \leftarrow 11_{1,11}$		3117.971	$11_{1,11} - 9_{19}$	44.885	0.000
$10_{28} \leftarrow 9_{27}$	A	3162.992[§]	$10_{28} \leftarrow 11_{29}$	A	3116.901	$11_{29} - 9_{27}$	46.091	−0.002
	E	3163.234		E	3117.142		46.092	−0.001
$10_{29} \leftarrow 9_{28}$		3163.112	$10_{29} \leftarrow 11_{2,10}$		3117.230	$11_{2,10} - 9_{28}$	45.882	0.003
$10_{37} \leftarrow 9_{36}$	A	3163.475	$10_{37} \leftarrow 11_{38}$	A	3117.573	$11_{38} - 9_{36}$	45.902	0.001
	E	3163.485[§]		E	3117.585		45.900	−0.001
$10_{38} \leftarrow 9_{37}$		3163.615	$10_{38} \leftarrow 11_{39}$		3117.720[§]	$11_{39} - 9_{37}$	45.896	−0.002
$10_4 \leftarrow 9_4$		3163.540	$10_4 \leftarrow 11_4$		3117.720[§]	$11_4 - 9_4$	45.820	−0.008
$10_5 \leftarrow 9_5$		3163.485[§]	$10_5 \leftarrow 11_5$		3117.746	$11_5 - 9_5$	45.739	−0.007
$11_{011} \leftarrow 10_{0,10}$ #		3165.358	$11_{010} \leftarrow 12_{0,12}$		3115.319	$12_{0,12} - 10_{0,10}$	50.038	−0.002
$11_{1,10} \leftarrow 10_{19}$		3165.915	$11_{1,10} \leftarrow 12_{1,11}$		3114.585	$12_{1,11} - 10_{19}$	51.330	−0.006
$11_{1,11} \leftarrow 10_{1,10}$	A	3164.860	$11_{1,11} \leftarrow 12_{1,12}$	A	3115.713	$12_{1,12} - 10_{1,10}$	49.147	0.000
	E	3164.712		E	3115.565		49.147	0.000
		*3165.256			*3116.110		49.146	0.000
$11_{29} \leftarrow 10_{28}$		3165.157	$11_{29} \leftarrow 12_{2,10}$		3114.647	$12_{2,10} - 10_{28}$	50.510	−0.008
$11_{2,10} \leftarrow 10_{29}$		3165.184	$11_{2,10} \leftarrow 12_{2,11}$		3114.949	$12_{2,11} - 10_{29}$	50.236	−0.003
$11_{39} \leftarrow 10_{38}$	A	3165.067	$11_{39} \leftarrow 12_{3,10}$	A	3114.798	$12_{3,10} - 10_{38}$	50.269	−0.002
	E	3165.285		E	3115.018		50.268	−0.003
$11_4 \leftarrow 10_4$		3165.439	$11_4 \leftarrow 12_4$		3115.256	$12_4 - 10_4$	50.183	−0.010
$12_{0,12} \leftarrow 11_{0,11}$ #	A	3167.150	$12_{0,12} \leftarrow 13_{0,13}$	A	3112.815[§]	$13_{0,13} - 11_{0,11}$	54.335	−0.001
	E	3167.274		E	3112.928		54.346	0.011
		*3167.001			*3112.67[§]		54.33	
$12_{1,11} \leftarrow 11_{1,10}$	A	3167.972	$12_{1,11} \leftarrow 13_{1,12}$	A	3112.190	$13_{1,12} - 11_{1,10}$	55.782	0.001
	E	3167.893		E	3112.112		55.782	0.001
$12_{1,12} \leftarrow 11_{1,11}$		3166.987	$12_{1,12} \leftarrow 13_{1,13}$	A	3113.590	$13_{1,13} - 11_{1,11}$	53.397	−0.008
$12_{2,10} \leftarrow 11_{29}$	A	3167.629	$12_{2,10} \leftarrow 13_{2,11}$	A	3112.681[§]	$13_{2,11} - 11_{29}$	54.949	−0.003
	E	3167.190[c]		E	3112.237[c]		54.954	0.002
$12_{2,11} \leftarrow 11_{2,10}$		3167.612	$12_{2,11} \leftarrow 13_{2,12}$		3113.006	$13_{2,12} - 11_{2,10}$	54.606	0.012
$12_{39} \leftarrow 11_{38}$	A	3167.540	$12_{39} \leftarrow 13_{3,10}$	A	3112.885	$13_{3,10} - 11_{38}$	54.655	0.000
	E	3167.657		E	3112.997		54.661	0.005
$12_{3,10} \leftarrow 11_{39}$		3167.446	$12_{3,10} \leftarrow 13_{3,11}$		3112.815[§]	$13_{3,11} - 11_{39}$	54.631	−0.014
$13_{0,13} \leftarrow 12_{0,12}$		3169.287	$13_{0,13} \leftarrow 14_{0,14}$		3110.667	$14_{0,14} - 12_{0,12}$	58.620	0.002
$13_{1,12} \leftarrow 12_{1,11}$		3169.839	$13_{1,12} \leftarrow 14_{1,13}$		3109.619	$14_{1,13} - 12_{1,11}$	60.220	−0.001
$13_{1,13} \leftarrow 12_{1,12}$	A	3168.897	$13_{1,13} \leftarrow 14_{1,14}$	A	3111.235	$14_{1,14} - 12_{1,12}$	57.661	0.002
	E	3168.939[c]		E	3111.278[c]		57.661	0.001
$13_{2,11} \leftarrow 12_{2,10}$		3169.433	$13_{2,11} \leftarrow 14_{2,12}$		3110.038	$14_{2,12} - 12_{2,10}$	59.395	0.000
		*3169.386			*3109.992		59.395	0.000
$13_{2,12} \leftarrow 12_{2,11}$	A	3169.293	$13_{2,12} \leftarrow 14_{2,13}$	A	3110.350	$14_{2,13} - 12_{2,11}$	58.943	−0.004
	E	3169.417		E	3110.468		58.949	0.001
$13_{3,11} \leftarrow 12_{3,10}$		3169.619	$13_{3,11} \leftarrow 14_{3,12}$		3110.600	$14_{3,12} - 12_{3,10}$	59.019	0.000
$13_4 \leftarrow 12_4$		3169.559[b]	$13_4 \leftarrow 14_4$		3110.643	$14_4 - 12_4$	58.916	−0.008
					3110.630			
$14_{0,14} \leftarrow 13_{0,13}$ #	A	3171.318	$14_{0,14} \leftarrow 15_{0,15}$	A	3108.430	$15_{0,15} - 13_{0,13}$	62.888	0.001
	E	3171.281		E	3108.394		62.887	0.000
$14_{1,13} \leftarrow 13_{1,12}$	A	3172.050	$14_{1,13} \leftarrow 15_{1,14}$	A	3107.391	$15_{1,14} - 13_{1,12}$	64.659	0.003
	E	3172.090		E	3107.433		64.657	0.001
$14_{1,14} \leftarrow 13_{1,13}$		3170.807	$14_{1,14} \leftarrow 15_{1,15}$		3108.898	$15_{1,15} - 13_{1,13}$	61.909	−0.002
$14_{2,12} \leftarrow 13_{2,11}$	A	3171.852	$14_{2,12} \leftarrow 15_{2,13}$	A	3108.009	$15_{2,13} - 13_{2,11}$	63.844	−0.003
	E	3171.643		E	3107.799		63.844	−0.002

TABLE 1 (Continued)

R			P			C.D.		δ
$14_{2,13} \leftarrow 13_{2,12}$		3171.546	$14_{2,13} \leftarrow 15_{2,14}$		3108.249	$15_{2,14} - 13_{2,12}$	63.297	0.000
$14_{3,11} \leftarrow 13_{3,10}$		*3171.795§	$14_{3,11} \leftarrow 15_{3,12}$		*3108.376	$15_{3,12} - 13_{3,10}$	63.419	0.004
		*3171.520			*3108.106		63.413	−0.002
		*3171.105			*3107.700		63.404	−0.011
$14_{3,12} \leftarrow 13_{3,11}$		3171.795§	$14_{3,12} \leftarrow 15_{3,13}$		3108.417	$15_{3,13} - 13_{3,11}$	63.378	−0.016
$14_4 \leftarrow 13_4$		3171.879	$14_4 \leftarrow 15_4$		3108.597	$15_4 - 13_4$	63.281	−0.008
$15_{0,15} \leftarrow 14_{0,14}$		3173.218	$15_{0,15} \leftarrow 16_{0,16}$		3106.078	$16_{0,16} - 14_{0,14}$	67.140	−0.001
$15_{1,14} \leftarrow 14_{1,13}$		3174.075	$15_{1,14} \leftarrow 16_{1,15}$		3104.995	$16_{1,15} - 14_{1,13}$	69.080	−0.004
$15_{1,15} \leftarrow 14_{1,14}$	A	3172.806	$15_{1,15} \leftarrow 16_{1,16}$	A	3106.647	$16_{1,16} - 14_{1,14}$	66.159	0.002
	E	3172.909		E	3106.751		66.158	0.000
$15_{2,13} \leftarrow 14_{2,12}$		3173.771	$15_{2,13} \leftarrow 16_{2,14}$		3105.465	$16_{2,14} - 14_{2,12}$	68.305	−0.002
$15_{2,14} \leftarrow 14_{2,13}$	A	3173.593	$15_{2,14} \leftarrow 16_{2,15}$	A	3105.946	$16_{2,15} - 14_{2,13}$	67.647	0.004
	E	3173.657		E	3106.012		67.645	0.002
$15_{3,12} \leftarrow 14_{3,11}$		3173.610	$15_{3,12} \leftarrow 16_{3,13}$		3105.810	$16_{3,13} - 14_{3,11}$	67.801	0.002
$15_{3,13} \leftarrow 14_{3,12}$		3173.620	$15_{3,13} \leftarrow 16_{3,14}$		3105.851	$16_{3,14} - 14_{3,12}$	67.769	0.000
$15_4 \leftarrow 14_4$		3173.283	$15_4 \leftarrow 16_4$		3105.632	$16_4 - 14_4$	67.651	−0.004
		3173.042			3105.394		67.649	−0.006
$16_{0,16} \leftarrow 15_{0,15}$	A	3175.349	$16_{0,16} \leftarrow 17_{0,17}$	A	3103.960	$17_{0,17} - 15_{0,15}$	71.390	0.006
	E	3175.398		E	3104.016		71.382	−0.001
$16_{1,15} \leftarrow 15_{1,14}$	A	3176.080	$16_{1,15} \leftarrow 17_{1,16}$	A	3102.572	$17_{1,16} - 15_{1,14}$	73.508	0.002
	E	3176.248		E	3102.740		73.508	0.001
$16_{1,16} \leftarrow 15_{1,15}$		3174.808	$16_{1,16} \leftarrow 17_{1,17}$		3104.406	$17_{1,17} - 15_{1,15}$	70.403	0.002
$16_{2,14} \leftarrow 15_{2,13}$	A	3175.306	$16_{2,14} \leftarrow 17_{2,15}$	A	3102.532	$17_{2,15} - 15_{2,13}$	72.775	−0.002
	E	3175.572		E	3102.798		72.775	−0.002
$16_{2,15} \leftarrow 15_{2,14}$		3175.365	$16_{2,15} \leftarrow 17_{2,16}$		3103.376	$17_{2,16} - 15_{2,14}$	71.989	0.003
$16_{3,13} \leftarrow 15_{3,12}$		3175.868	$16_{3,13} \leftarrow 17_{3,14}$		3103.685	$17_{3,14} - 15_{3,12}$	72.183	−0.002
		3176.122			3103.939		72.183	−0.001
		3175.662			3103.478		72.184	−0.001
$16_4 \leftarrow 15_4$		3175.803[b]	$16_4 \leftarrow 17_4$		3103.788[b]	$17_4 - 15_4$	72.015	−0.007
$17_{0,17} \leftarrow 16_{0,16}$		3177.175	$17_{0,17} \leftarrow 18_{0,18}$		3101.561[d]	$18_{0,18} - 16_{0,16}$	75.614	0.003
$17_{1,16} \leftarrow 16_{1,15}$		3178.065	$17_{1,16} \leftarrow 18_{1,17}$		3100.149	$18_{1,17} - 16_{1,15}$	77.916	−0.004
$17_{1,17} \leftarrow 16_{1,16}$	A	3176.513	$17_{1,17} \leftarrow 18_{1,18}$	A	3101.872	$18_{1,18} - 16_{1,16}$	74.641	0.001
	E	3176.744		E	3102.103		74.641	0.001
$17_{2,15} \leftarrow 16_{2,14}$		3177.770	$17_{2,15} \leftarrow 18_{2,16}$		3100.516	$18_{2,16} - 16_{2,14}$	77.255	0.000
$17_{2,16} \leftarrow 16_{2,15}$	A	3177.387	$17_{2,16} \leftarrow 18_{2,17}$	A	3101.055	$18_{2,17} - 16_{2,15}$	76.332	0.007
	E	3177.329		E	3100.999		76.330	0.006
$17_{3,14} \leftarrow 16_{3,13}$		3177.865§	$17_{3,14} \leftarrow 18_{3,15}$		3101.312	$18_{3,15} - 16_{3,13}$	76.565	−0.009
$17_{3,15} \leftarrow 16_{3,14}$	A	3177.937	$17_{3,15} \leftarrow 18_{3,16}$	A	3101.417	$18_{3,16} - 16_{3,14}$	76.519	0.001
	E	3177.691		E	3101.169		76.522	0.004
$17_4 \leftarrow 16_4$		3177.474	$17_4 \leftarrow 18_4$		3101.090	$18_4 - 16_4$	76.384	−0.004
$18_{0,18} \leftarrow 17_{0,17}$	A	3179.076	$18_{0,18} \leftarrow 19_{0,19}$	A	3099.244	$19_{0,19} - 17_{0,17}$	79.831	0.004
	E	3178.948		E	3099.115		79.833	0.005
$18_{1,17} \leftarrow 17_{1,16}$	A	3180.176	$18_{1,17} \leftarrow 19_{1,18}$	A	3097.847	$19_{1,18} - 17_{1,16}$	82.330	0.003
	E	3180.079		E	3097.746		82.334	0.007
$18_{1,18} \leftarrow 17_{1,17}$		3178.787	$18_{1,18} \leftarrow 19_{1,19}$		3099.908	$19_{1,19} - 17_{1,17}$	78.879	0.005
		*3178.560			*3099.678		78.882	0.008
$18_{2,16} \leftarrow 17_{2,15}$		3179.386	$18_{2,16} \leftarrow 19_{2,17}$		3097.659	$19_{2,17} - 17_{2,15}$	81.727	−0.012
$18_{2,17} \leftarrow 17_{2,16}$		3179.343	$18_{2,17} \leftarrow 19_{2,18}$		3098.684	$19_{2,18} - 17_{2,16}$	80.659	0.000
$18_{3,15} \leftarrow 17_{3,14}$		3179.815	$18_{3,15} \leftarrow 19_{3,16}$		3098.853	$19_{3,16} - 17_{3,14}$	80.963	−0.003
$19_{0,19} \leftarrow 18_{0,18}$		3181.019§	$19_{0,19} \leftarrow 20_{0,20}$		3096.990	$20_{0,20} - 18_{0,18}$	84.029	−0.003
$19_{1,18} \leftarrow 18_{1,17}$		3182.282	$19_{1,18} \leftarrow 20_{1,19}$		3095.555	$20_{1,19} - 18_{1,17}$	86.727	0.002
$19_{1,19} \leftarrow 18_{1,18}$		3180.545	$19_{1,19} \leftarrow 20_{1,20}$		3097.441	$20_{1,20} - 18_{1,18}$	83.104	0.000
		3180.318			3097.218		83.099	−0.005
		*3180.579			*3097.478		83.101	−0.003
$19_{2,18} \leftarrow 18_{2,17}$	A	3181.129	$19_{2,18} \leftarrow 20_{2,19}$	A	3096.129	$20_{2,19} - 18_{2,17}$	84.999	0.011
	E	3181.019§		E	3096.013		85.006	0.018
$19_{3,17} \leftarrow 18_{3,16}$		3181.462	$19_{3,17} \leftarrow 20_{3,18}$		3096.192	$20_{3,18} - 18_{3,16}$	85.270	0.003
$19_4 \leftarrow 18_4$		3181.523[b]	$19_4 \leftarrow 20_4$		3096.410[e]	$20_4 - 18_4$	85.113	−0.010
$20_{0,20} \leftarrow 19_{0,19}$	A	3182.843	$20_{0,20} \leftarrow 21_{0,21}$	A	3094.617[f]	$21_{0,21} - 19_{0,19}$	88.226	0.002
	E	3182.854		E	3094.627		88.227	0.002
$20_{1,19} \leftarrow 19_{1,18}$	A	3184.091	$20_{1,19} \leftarrow 21_{1,20}$	A	3092.972	$21_{1,20} - 19_{1,18}$	91.119	0.005
	E	3184.030		E	3092.911		91.119	0.006
$20_{1,20} \leftarrow 19_{1,19}$		3182.489	$20_{1,20} \leftarrow 21_{1,21}$		[g]			
$20_{2,18} \leftarrow 19_{2,17}$		3183.917	$20_{2,18} \leftarrow 21_{2,19}$		3093.192	$21_{2,19} - 19_{2,17}$	90.725	−0.001
$20_{2,19} \leftarrow 19_{2,18}$		3183.189	$20_{2,19} \leftarrow 21_{2,20}$		3093.863	$21_{2,20} - 19_{2,18}$	89.326	0.013
$21_{1,20} \leftarrow 20_{1,19}$		3186.013	$21_{1,20} \leftarrow 22_{1,21}$		3090.515	$22_{1,21} - 20_{1,19}$	95.498	0.007
$21_{1,21} \leftarrow 20_{1,20}$		3184.400	$21_{1,21} \leftarrow 22_{1,22}$		3092.838	$22_{1,22} - 20_{1,20}$	91.561	0.010
$21_{2,20} \leftarrow 20_{2,19}$		3185.163	$21_{2,20} \leftarrow 22_{2,21}$		3091.524§	$22_{2,21} - 20_{2,19}$	93.639	0.006
$21_{3,19} \leftarrow 20_{3,18}$		3185.533	$21_{3,19} \leftarrow 22_{3,20}$		3091.524§	$22_{3,20} - 20_{3,18}$	94.010	−0.003
$22_{0,22} \leftarrow 21_{0,21}$	A	3186.659	$22_{0,22} \leftarrow 23_{0,23}$	A	3090.081	$23_{0,23} - 21_{0,21}$	96.578	−0.002
	E	3186.625		E	3090.046		96.579	−0.002
$22_{1,21} \leftarrow 21_{1,20}$	A	3187.994	$22_{1,21} \leftarrow 23_{1,22}$	A	3088.130	$23_{1,22} - 21_{1,20}$	99.864	0.005
	E	3188.135		E	3088.263		99.872	0.013
$22_{1,22} \leftarrow 21_{1,21}$		3186.200	$22_{1,22} \leftarrow 23_{1,23}$		3090.430	$23_{1,23} - 21_{1,21}$	95.771	0.002
$22_{2,20} \leftarrow 21_{2,19}$		3188.123§	$22_{2,20} \leftarrow 23_{2,21}$		3088.412	$23_{2,21} - 21_{2,19}$	99.711	−0.015

TABLE 1 (Continued)

R		P		C.D.		δ
$23_{0,23} \leftarrow 22_{0,22}$	3188.427	$23_{0,23} \leftarrow 24_{0,24}$	3087.683	$24_{0,24} - 22_{0,22}$	100.744	−0.003
$23_{1,22} \leftarrow 22_{1,21}$	(3190.066)§	$23_{1,22} \leftarrow 24_{1,23}$	*h*			
$23_{1,23} \leftarrow 22_{1,22}$	3188.123§	$23_{1,23} \leftarrow 24_{1,24}$	3088.139	$24_{1,24} - 22_{1,22}$	99.984	0.003
$23_{2,22} \leftarrow 22_{2,21}$	3188.998	$23_{2,22} \leftarrow 24_{2,23}$	3086.728	$24_{2,23} - 22_{2,21}$	102.270	0.014
$24_{0,24} \leftarrow 23_{0,23}$	3190.066§	$24_{0,24} \leftarrow 25_{0,25}$	3085.160	$25_{0,25} - 23_{0,23}$	104.906	0.000
$24_{1,23} \leftarrow 23_{1,22}$	3191.874	$24_{1,23} \leftarrow 25_{1,24}$	3083.310	$25_{1,24} - 23_{1,22}$	108.565	0.006
$24_{2,22} \leftarrow 23_{2,21}$	3191.850	$24_{2,22} \leftarrow 25_{2,23}$	3083.127	$25_{2,23} - 23_{2,21}$	108.723	−0.006

[a] The position of this transition is anomalous, but this is the only way to satisfy the combination difference and intensity. [b] A broad line. [c] The intensity of the E component is anomalously weak compared to the A component. [d] Anomalously weak. [e] Overlapped with H_3^+ R(5,5)$^+$. [f] Overlapped with HCO^+ R(1). [g] Overwhelmed by CH_4 R(7) $F_1^{(2)} \leftarrow F_2^{(1)}$. [h] Overwhelmed by CH_4 R(6) $F_1^{(1)} \leftarrow F_1^{(0)}$. [i] *Extra lines assignable to the indicated transition. § More than one transition of $C_2H_3^+$ is assignable at this frequency. The sign indicates the more tentative assignment(s). # Misassigned in ref 10.

forward current of 0.5 A. To ensure that the cathode does not conduct on the reverse half-cycle, we placed a diode and a 1 kΩ resistor in parallel with the hollow cathode to conduct on the negative half-cycles and thus reduce the anode voltage below the breakdown level at these times. We achieved a peak current of 1.75 A on the conducting half-cycles. The plasma was cooled with tap water flowing through tubes soldered onto the outside of the cathode.

3. Observed Spectrum

We recorded spectra of the C_2H_2/H_2 hollow cathode plasma from 3205 to 3070 cm^{-1} with our difference-frequency spectrometer. As earlier shown by Amano, the lines in our spectrum appeared to be due almost exclusively to $C_2H_3^+$ except for some from other protonated ions such as the necessary H_3^+ and the protonated impurities HN_2^+, HCO^+, and $HCNH^+$. All known lines of the fragmentary ions CH_3^+ and CH_2^+ and the primary ion $C_2H_2^+$, which are often stronger than those of $C_2H_3^+$ in positive column discharges, are almost totally absent. A comparison of spectra recorded through the hollow cathode and those from a positive column discharge is given in Figure 2. The purity of the $C_2H_3^+$ spectrum in the hollow cathode plasma is striking. Such dominance of the $C_2H_3^+$ spectral lines has allowed us to clarify the carbocation spectra considerably.

We have extended our assignment to higher J values (up to $J = 25$) and higher K_a values (up to $K_a = 4$). As mentioned in our earlier paper,[10] the anomalous spectral pattern did not allow us to assign spectral lines by fitting the transitions to asymmetric rotor levels. We instead relied on ground state combination differences calculated from the appropriate R and P branch lines and the spin statistical weight of 2:1. Compared with our previous result, we could conduct this process with much greater confidence because of (a) the purity of the $C_2H_3^+$ spectrum and thus the lack of overlapping CH_3^+ and $C_2H_2^+$ lines and (b) the available more accurate combination differences from the millimeter wave spectrum.[26] The assigned lines are listed in Tables 1 and 2. Since the assignment is based almost exclusively on combination differences, the spectral lines in Tables 1 and 2 are arranged such that combination differences are explicit. Our new result has revealed some misassignment in our earlier paper;[10] while all transitions with $K_a = 1$ were correctly assigned, some transitions with $K_a = 0$ and 2 needed to be reassigned. These transitions are indicated with a # in Table 1. While we cannot completely eliminate the possibility that some pairs of spectral lines accidentally satisfy the ground state combination differences and thus are incorrectly assigned, we believe that most of the assignments are correct. Where combination differences indicate that two transitions fall at the same frequency and the assignment of the line to one of them is for any reason less certain, we have marked that entry in Table 1 with a §. The discrepancies between observed and calculated values of the ground state combination differences are listed in the last column of Tables 1 and 2 as δ.

The rotational and centrifugal distortion constants used in the calculation are listed in Table 3. Watson's *A*-reduced Hamiltonian[39] has been used in the least squares fit of the observed combination differences together with the millimeter wave transitions from ref 26. The determined rotational constants are very close to those given in ref 26.

To separate A and Δ_K, the value of the latter was calculated by a normal coordinate calculation from the formulas[39]

$$-\Delta_K = T_{aa} + \Delta_J + \Delta_{JK}$$

$$T_{aa} = -A^3 \sum_s \frac{(a_s^{aa})^2}{I_{aa}} \frac{1}{\upsilon_s^2}$$

where A is the rotational constant. $a_s^{aa} \equiv (\partial I_{aa}/\partial Q_s)$ is the derivative of the moment of inertia I_{aa} with respect to the normal coordinate Q_s, and s runs over the totally symmetric normal modes 1−4. Vibrational frequencies υ_s predicted by Schaefer and co-workers[40] from *ab initio* calculations are used. Using the calculated value of $\Delta_K = 0.00144(15)$ cm^{-1} and ignoring $\delta_K \sim 2 \times 10^{-5}$ cm^{-1}, individual rotational constants were derived as shown in Table 3, where the uncertainties of B and C are estimated from the absolute value of the neglected δ_K. The small positive inertial defect Δ_0 clearly indicates the planarity of the $C_2H_3^+$ frame.

Even for those $C_2H_3^+$ lines that could not be assigned, the hollow cathode spectrum has clearly identified their carrier to be $C_2H_3^+$. In view of the existence of low-frequency vibrations[40] such as the υ_5 antisymmetric out-of-plane CH bending vibration or the υ_8 antisymmetric in-plane CH bending vibration, which are predicted at 587 and 513 cm^{-1}, respectively,[40] the presently unassigned lines are likely to be hot band transitions. On the other hand, the many weak lines in the upper trace of Figure 2 that are not in the lower trace are due to carbocations other than $C_2H_3^+$; such clear discrimination will greatly help future studies of carbocation spectra.

4. Spectral Splitting Due to Proton Tunneling

As discussed extensively in ref 10, the three protons of $C_2H_3^+$ undergo a tunneling motion among their equilibrium positions on a time scale sufficiently short that the resulting splitting of spectral lines is observable. The splitting is up to 0.4 cm^{-1} (~100 ps) in the υ_6 excited state[10] and is less than 1 MHz (~1 μs) in the ground vibrational state.[26] To discuss the symmetry of quantum states under such motion, we used in ref 10 the complete permutation inversion group $G_{24} = S_2 \otimes S_3 \otimes E^*$, where S_2 and S_3 are symmetry groups for permutation of the two carbon atoms and the three protons, respectively, and E^*

TABLE 2: Q Branch Lines and Combination Differences (in cm^{-1}), δ = (C.D.)$_{obs}$ − (C.D.)$_{calc}$

Q			P, R			C.D.		δ
$2_{11} \leftarrow 2_{12}$		3142.526	$2_{11} \leftarrow 3_{12}$		3135.536	$3_{12} - 2_{12}$	6.989	−0.005
			$2_{11} \leftarrow 1_{10}$		3146.713	$2_{12} - 1_{10}$	4.179	−0.006
$2_{20} \leftarrow 2_{21}$		3141.957	$2_{20} \leftarrow 3_{21}$		3135.395	$3_{21} - 2_{21}$	6.562	−0.001
$3_{13} \leftarrow 3_{12}$		3141.442	$3_{13} \leftarrow 4_{14}$		3133.458	$4_{14} - 3_{12}$	7.984	−0.003
			$3_{13} \leftarrow 2_{12}$		3148.439	$3_{12} - 2_{12}$	6.998	0.004
$3_{21} \leftarrow 3_{22}$		3141.647	$3_{21} \leftarrow 4_{22}$		3132.894	$4_{22} - 3_{22}$	8.753	−0.002
			$3_{21} \leftarrow 2_{20}$		3148.211	$3_{22} - 2_{20}$	6.564	0.004
$3_{22} \leftarrow 3_{21}$		3141.124	$3_{22} \leftarrow 4_{23}$		3132.379	$4_{23} - 3_{21}$	8.745	0.001
			$3_{22} \leftarrow 2_{21}$		3147.684	$3_{21} - 2_{21}$	6.559	−0.004
$3_3 \leftarrow 3_3$		3142.023	$3_3 \leftarrow 4_3$		3133.286	$4_3 - 3_3$	8.738	−0.003
		3142.019			3133.286		8.733	−0.007
$4_{22} \leftarrow 4_{23}$		3142.092	$4_{22} \leftarrow 5_{23}$		3131.140	$5_{23} - 4_{23}$	10.952	−0.001
			$4_{22} \leftarrow 3_{21}$		3150.839	$4_{23} - 3_{21}$	8.747	0.003
$4_{23} \leftarrow 4_{22}$		3141.554	$4_{23} \leftarrow 5_{24}$		3130.630	$5_{24} - 4_{22}$	10.924	−0.001
			$4_{23} \leftarrow 3_{22}$		3150.310	$4_{22} - 3_{22}$	8.756	0.001
$4_3 \leftarrow 4_3$		3141.999	$4_3 \leftarrow 5_3$		3131.072	$5_3 - 4_3$	10.927	0.002
			$4_3 \leftarrow 3_3$		3150.736	$4_3 - 3_3$	8.737	−0.003
$4_4 \leftarrow 4_4$		3142.121[a]						
$5_{24} \leftarrow 5_{23}$	A	3141.729	$5_{24} \leftarrow 4_{23}$	A	3152.682	$5_{23} - 4_{23}$	10.954	0.002
	E	3141.361		E	3152.313		10.952	0.000
$5_3 \leftarrow 5_3$	A	3141.904	$5_3 \leftarrow 6_3$	A	3128.803	$6_3 - 5_3$	13.101	−0.010
	E	3142.132		E	3129.024		13.108	−0.003
$5_4 \leftarrow 5_4$		3142.187	$5_4 \leftarrow 6_4$		3129.104	$6_4 - 5_4$	13.083	−0.010
		3142.260			3129.170		13.089	−0.004
			$5_4 \leftarrow 4_4$		3153.100	$5_4 - 4_4$	10.913	0.002
					3153.171		10.911	0.001
$5_5 \leftarrow 5_5$		3142.220[a]						

[a] No ground state combination difference because of weak P and Q branch lines.

TABLE 3: Rotational Constants in the Ground Vibrational State Calculated from a Least Squares Fit of Observed Infrared Combination Differences and the Microwave Transitions Listed in Ref 26 (in cm^{-1} Except Where Noted)

Determined Constants	
$A - \Delta_K$	13.3410974(81)[a]
$(B + C)/2$	1.0942438(37)
$(B - C)/4 - \delta_K$	0.02389801(67)
Δ_J	$1.256(15) \times 10^{-6}$
Δ_{JK}	$2.0145(69) \times 10^{-4}$
δ_J	$1.047(24) \times 10^{-7}$
Derived Constants	
A	13.33966(15)
B	1.14204(2)
C	1.04645(2)
Δ_K	0.00144(15)
Δ_0	0.0847 amu Å^2

[a] Values in parentheses are 1σ.

= $\{E, E^*\}$ is the space inversion group composed of the identity E and the space inversion operation E^*. Since the carbon nucleus is a boson with spin 0, however, only states that are totally symmetric with respect to S_2 are allowed (g states in ref 10). Therefore, we can use a smaller group $G_{12} = S_3 \otimes E^*$, which is isomorphic to D_{3h}, to fully describe the symmetry of levels and the selection rules for transitions.

As shown in ref 10, the effect of the proton tunneling is to split the (K_a, K_c) = (even, odd) or (o, e) levels in the ground state and the (e, e) and (o, o) levels in the excited state with a spin statistical weight of 3 in a rigid molecule into two components, A_2 and E, with spin statistical weights of 2 and 1, respectively. The (K_a, K_c) = (e,e) or (o,o) levels in the ground state and the (e,o) or (o,e) levels in the excited state with a spin statistical weight of 1 are not affected. Thus instead of the two-proton ortho−para statistical weight of 3 to 1, we now have the three-proton ortho−para statistical weight of 4 to 2 to 2.

Since the tunneling splitting in the ground vibrational state ($\Delta\nu \lesssim 1$ MHz)[29] is much smaller than the resolution of our Doppler-limited spectroscopy, the tunneling effect appears as identical splittings in the corresponding R and P branch transitions which share the same split upper levels. Examples of pairs of transitions between $K_a = 0$ rotational levels are shown in Figure 3. Observed splittings for $K_a = 0-3$ rotational levels are listed in Table 4. The splittings in the excited states are on the order of 0.1 cm^{-1} and are up to 0.44 cm^{-1}, 4 orders of magnitude higher than the splittings in the ground state. The variation of the tunneling splitting with J is plotted in Figure 4. We do not see any obvious regularity in the splitting. Sometimes levels are split into more than two components. Also, even when the level splits into two, the intensity ratio is not always 2:1. These complications must arise from mixing of the A and/or E levels with some dark states with the same symmetry which happen to lie close in energy. With the existence of low-frequency vibrations in $C_2H_3^+$, there are plenty of candidates for such states. Extra lines due to this effect are marked with an * in Table 1. Some vibrational modes which couple strongly with proton tunneling may split the A and E levels far apart.

The orders of magnitude increase on the tunneling splittings in the excited state compared with those in the ground state is surprising in view of the fact that the C−H antisymmetric ν_6 mode does not couple with the proton-tunneling motion directly. The increase is probably explained as due to a small mixing of the ν_6 state with higher harmonics of bending vibrations such as ν_8, which couples strongly with the tunneling motion. This effectively lowers the barrier of tunneling; the height of such an effective barrier may be determined from the observed A−E splitting. We hope that the observed splittings shown in Table 4 and Figure 3 will be quantitatively explained some day.

5. Plasma Chemistry in the Hollow Cathode Discharge

Like Amano's earlier works,[15-22] our results clearly demonstrate that the molecular ion population in the hollow cathode discharge is dominated by protonated ions. This is in sharp contrast to the case of our He-dominated positive column discharges, in which large amounts of carbocations containing one carbon atom, such as CH_3^+ and CH_2^+, are produced in

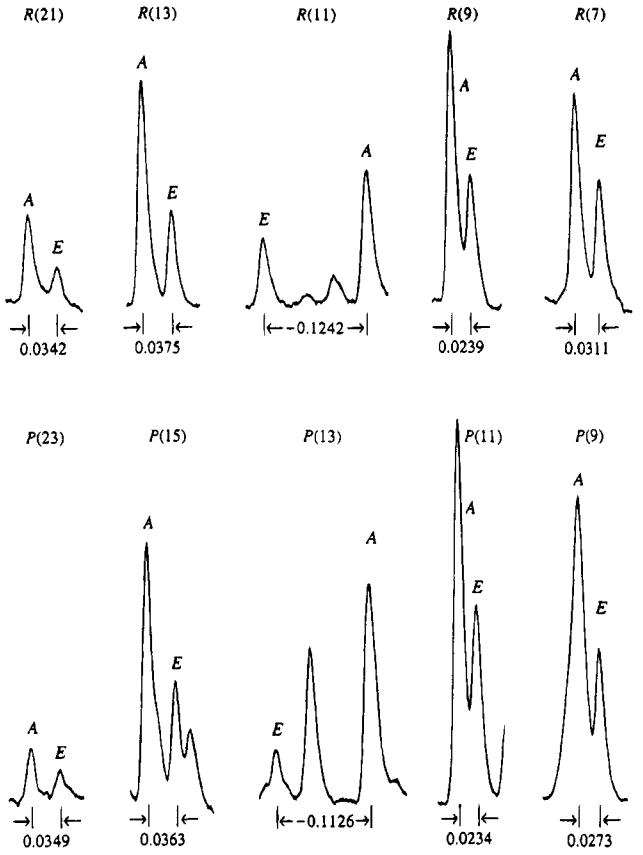

Figure 3. A−E splittings of ortho $C_2H_3^+$ rotational levels with K_a = 0 due to the tunneling of the three protons among their equilibrium positions. Since the splitting in the ground vibrational state is small (<1 MHz),[29] the observed splittings are due to the upper levels, and the P and R transitions with a common upper level show the same splitting. Because of the irregular $J_{Ka,Kc}$ dependence of the splitting, the assignment is based on the identical P and R splittings and the approximate A/E = 2/1 intensity ratio.

discharges containing acetylene. In this section we attempt to analyze the plasma chemistry in hollow cathode discharges.

A. Background. The hollow cathode discharge was introduced by Paschen[41] based on his accidental discovery in 1914 with H. Bartels that atomic emission lines were very strong in the bright layer inside the cylindrical cathode of their He-filled Geissler tube. His first hollow cathode discharge,[41] used for the study of the hydrogen-like emission spectrum of He^+, which played a key role in establishing the Sommerfeld fine-structure formula, had all the essential features of the hollow cathode discharge. According to Tolansky,[42] "The very many later modifications which have been introduced are improvements in detail without alteration in the essential discharge conditions realized by him." Schüler[43] measured the electric field in his hollow cathode discharge and found it to be very much lower than that in a positive column glow discharge. This low field provided sharp spectral lines essentially free from Stark broadening; the low electron temperature also kept the gas temperature low, leading to small Doppler broadening. These characteristics of hollow cathode discharges enabled him to observe the fine structure of the Li^+ spectrum,[44] which provided supporting evidence for Heisenberg's theory of ortho and para helium. Schüler[45] altered the design of the cell by bringing the cathode outside of the discharge so that the cathode could be cooled by water or liquid nitrogen and used it for his extensive studies of the hyperfine structure of atomic spectra. The low electric field and the resulting low temperature of electrons and hence of the whole plasma are the crucial features of a hollow cathode discharge, which sometimes is also called a Schüler discharge.[46]

TABLE 4: $A-E$ Splitting in the ν_6 Excited State of $C_2H_3^+$ Due to Proton Tunneling (in cm^{-1}), $\Delta = E_A - E_E$

$K_a = 0$

$J_{0,J}$	R	P	$\Delta_{av.}$
2_{02}	0.3400	0.3384	0.339
4_{04}	0.0729	0.0674	0.070
6_{06}	−0.1038	−0.1078	−0.106
8_{08}	0.0311	0.0273	0.029
$10_{0,10}$	0.0239	0.0234	0.024
$12_{0,12}$	−0.1242	−0.1126	−0.118
$14_{0,14}$	0.0375	0.0363	0.037
$16_{0,16}$	−0.0488	−0.0566	−0.053
$18_{0,18}$	0.1279	0.1293	0.129
$20_{0,20}$	−0.0113	−0.0104	−0.011
$22_{0,22}$	0.0342	0.0349	0.035

$K_a = 1$

J_{1,K_c}	R	P	$\Delta_{av.}$
2_{11}	0.2051	0.2103	0.208
3_{13}	−0.4110	−0.4108	−0.411
*	−0.3761	−0.3721	−0.374
4_{13}	0.0572	0.0537	0.055
5_{15}	−0.0386	−0.0363	−0.037
6_{15}	−0.0601	−0.0606	−0.060
7_{17}	0.0976	0.0997	0.099
8_{17}	0.0193	0.0184	0.019
9_{19}	0.2998	0.3011	0.300
*	0.4736	0.4763	0.475
10_{19}	0.0569	0.0546	0.056
$11_{1,11}$	0.1475	0.1475	0.148
$12_{1,11}$	0.0790	0.0786	0.079
$13_{1,13}$	−0.0420	−0.0424	−0.042
$14_{1,13}$	−0.0400	−0.0420	−0.041
$15_{1,15}$	−0.1027	−0.1042	−0.103
$16_{1,15}$	−0.1674	−0.1679	−0.168
$17_{1,17}$	−0.2312	−0.2312	−0.231
$18_{1,17}$	0.0972	0.1012	0.099
$19_{1,19}$	0.2264	0.2224	0.224
*	−0.0345	−0.0374	−0.036
$20_{1,19}$	0.0611	0.0615	0.061
$22_{1,21}$	−0.1408	−0.1330	−0.137

$K_a = 2$

J_{2,K_c}	R	P	$\Delta_{av.}$
4_{22}	0.2865	0.2813	0.284
*	0.5863	0.5851	0.586
5_{24}	0.3696	0.3719	0.371
6_{24}	−0.3133	−0.3105	−0.312
7_{26}	0.0502	0.0468	0.049
8_{26}	−0.1483	−0.1485	−0.148
*	−0.2081	−0.2080	−0.208
9_{28}	0.1616	0.1623	0.162
10_{28}	−0.2419	−0.2411	−0.242
$12_{2,10}$	0.4389	0.4439	0.441
$13_{2,12}$	−0.1237	−0.1183	−0.121
$14_{2,12}$	0.2091	0.2095	0.209
$15_{2,14}$	−0.0641	−0.0662	−0.065
$16_{2,14}$	−0.2659	−0.2659	−0.266
$17_{2,16}$	0.0577	0.0562	0.057
$19_{2,18}$	0.1098	0.1168	0.113

$K_a = 3$

J_{3,K_c}	R	P	$\Delta_{av.}$
5_3	−0.2241	−0.2207	−0.222
6_3	0.0566	0.0595	0.058
9_{37}	0.1769	0.1762	0.177
10_{37}	−0.0102	−0.0123	−0.011
11_{39}	−0.2178	−0.2191	−0.218
12_{39}	−0.1167	−0.1114	−0.114

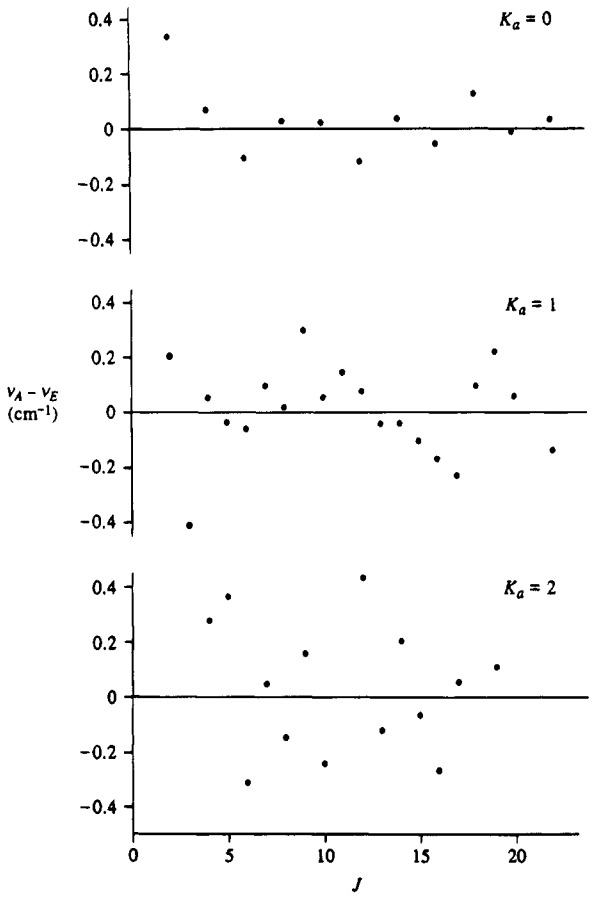

Figure 4. Plot of the observed A−E splittings for $K_a = 0$, 1, and 2 as a function of J in the ν_6 excited state. The data for these graphs are given in Table 3. We can see no pattern in the magnitude of the splittings vs J. Very generally, the magnitude increases with K_a.

The hollow cathode discharge for emission spectroscopy has recently made a spectacular comeback in Herzberg's discovery of the H_3 and D_3 emission spectra.[47−49] Using a modified design of Schüler's liquid-nitrogen-cooled hollow cathode cell,[50] Herzberg and his colleagues noted that such a discharge is a unique light source for the H_3 emission spectrum. Also noteworthy is the work of Majewski, Watson, and others,[51,52] who observed the infrared emission spectrum of H_3^+ using a copper hollow cathode with a small bore similar in design to the hollow cathode of Paschen and Ritschl.[53]

Quite apart from these applications for emission spectroscopy, hollow cathode discharges, rich in molecular ions, provide a useful medium for absorption spectroscopy when combined with intense tunable radiation sources. Van den Heuvel and Dymanus[37] seem to have been the first to have used a hollow cathode for molecular ions and observed with it far infrared spectra of HCO^+, CO^+, and HN_2^+. Their symmetric design, in which the anode is placed at the midpoint above the cathode tube, has been adopted by Foster, McKellar, and Sears[38] and by Amano.[14−22] Our hollow cathode also follows this design but is more similar to Schüler's original in that the cathode is outside and its outer wall is exposed to the air.

B. Electrons in the Plasma. *B.1. Ultimate Electrons and Recombination.* The inner bulk of a hollow cathode discharge may be considered to be coalesced negative glow,[46,54,55] where the electric field is very low ($E < 1$ V/cm), as initially reported by Schüler.[43] It is surrounded by the cathode dark space, where the electric field varies approximately linearly with the distance from the cathode surface from the high value of several hundred volts/centimeter at the cathode to a low value at the boundary of the cathode dark space and negative glow.

Diagnostic studies of electrons in the negative glow have been reported in many papers (see ref 46 and ref 56−62 and references therein). While the results differ quantitatively for different gases and different plasma conditions, it is well established that electrons in the negative glow are composed of a majority of low-temperature electrons and a small fraction (≈1%) of hot electrons. Langmuir[63] classified electrons in any plasma into three categories: (i) the primary electrons ejected from the cathode and accelerated by the large cathode fall to several tens of electronvolts, (ii) the secondary electrons with an energy of several electronvolts ejected from gases due to ionization by the primary electrons, and (iii) the "ultimate" electrons traveling at low energy, which are the end state of secondary electrons that have lost their energy after many collisions.

The special characteristics of the negative glow and hence the hollow cathode discharge as a chemical environment is that the temperature of the ultimate electrons is orders of magnitude less than in the positive glow. Temperatures of 400,[57] 600,[58] 500,[60] and 1000 K[61] have been reported, in sharp contrast to the typical electron temperature in positive column discharges of several electronvolts.[54] The negative charge of the low-temperature electrons balances the positive charge of molecular cations and allows the latter to exist abundantly in hollow cathode discharges. Since the average kinetic energy of such electrons is far too low to ionize or dissociate neutral molecules, the only chemical reaction in which these electrons are involved is the dissociative recombination of cations, in which they play the dominant role due to their abundance.

The dissociative recombination rate of H_3^+ has been the subject of considerable controversy during the past decade.[64,65] The initially well-accepted value for the rate constant of 2.3×10^{-7} cm^3 s^{-1} reported by Leu, Biondi, and Johnsen[66] was reduced to less than 2×10^{-11} cm^3 s^{-1} by Adams and Smith.[67,68] However, starting from Amano's spectroscopic study using a hollow cathode discharge,[69,70] a consensus seems to have been reached for a value on the order of 10^{-7} cm^3 s^{-1} by several groups using different experimental methods,[71−74] although some controversy still remains.[75−77] In the following calculations we use Amano's recombination rate constant $k_r = 1.8 \times 10^{-7}$ cm^3 s^{-1} because of the similarity between his and our plasmas. For the recombination of $C_2H_2^+$ and $C_2H_3^+$, we use the rate constants $k_r = 2.7 \times 10^{-7}$ and 4.5×10^{-7} cm^3 s^{-1}, respectively, reported by Mul and McGowan.[78] In view of the fact that the electron temperature is not greatly different from room temperature, the temperature variation $\sim(300/T)^{0.5}$ of the rate constant is neglected.

B.2. Hot Electrons and Ionization. The ionization of molecules is effected by the primary and secondary electrons, which are together called hot electrons.[62] On the basis of previous diagnostics[56−58,61,62] of electrons in the negative glow, we assume the average energy E_m of the primary electrons to be 40 eV and that of the secondary electrons to be 4 eV. The latter is much less than the ionization potentials of H_2 (15.43 eV) and C_2H_2 (11.41 eV), and therefore ionization is carried out by electrons in the high-energy tail of the electron energy distribution. The energy distributions of both types of electrons are assumed to be Boltzmannian,[54]

$$dN = (2n_e/\sqrt{\pi})\sqrt{E/E_m}\,e^{-E/E_m}\,d(E/E_m)$$

where n_e is the number density of electrons for each category of electrons; their assumed values will be given in section 5C.

The ionization rate constants are calculated by

$$k_i = (1/n_e)\int \sigma(E) v \, dN$$

where $\sigma(E)$ is the energy-dependent ionization cross section and the velocity $v = (E/E_m)^{1/2} v_m$ with the mean velocity $v_m = (2E_m/m)^{1/2}$.

Using these formulas along with the values of $\sigma(E)$ reported for H_2 by Rapp and Englander-Golden[79,80] and those for C_2H_2 by Tate and Smith,[81] we calculate the values of $k_i = 3.10 \times 10^{-10}$ and 2.80×10^{-8} cm^3 s^{-1} for H_2 and $k_i = 2.52 \times 10^{-9}$ and 1.52×10^{-7} cm^3 s^{-1} for C_2H_2 for secondary electrons with an energy of 4 eV and for primary electrons with an energy of 40 eV, respectively. Gaudin and Hagemann[82] studied cross sections of C_2H_2 ionization producing $C_2H_2^+$ and those of dissociative ionization producing C_2H^+ and C_2^+; the values of $\sigma(E)$ for the two dissociative processes are smaller than that for simple ionization by factors of 7 and 20, respectively. The consequences of the latter reactions are lumped into the ionization leading to $C_2H_2^+$ in view of the smallness of their cross sections and the efficiency of the hydrogen abstraction reactions,[83]

$$C_2^+ \xrightarrow[-H]{H_2} C_2H^+ \xrightarrow[-H]{H_2} C_2H_2^+$$

The $\sigma(E)$ values given by Rapp and Englander-Golden contain these results.

Gaudin and Hagemann's cross sections for the dissociative ionizations of acetylene in which the C≡C bond is broken to produce CH^+ or C^+ are 2 orders of magnitude smaller than that for the ionization leading to $C_2H_2^+$. We neglect these reactions in our model calculation. The smallness of these cross sections explains the absence of the spectra of carbocations with one carbon atom such as CH_2^+ and CH_3^+. This is in sharp contrast to He-dominated positive column discharges, in which the C≡C bond of acetylene is efficiently broken through Penning dissociative ionization.

C. Ion–Neutral Reactions and Chemical Equilibrium. The observed optimum gas mixture of $H_2/C_2H_2 = 1.1/0.03$ Torr for the spectrum of $C_2H_3^+$ and the nearly total absence of lines due to CH_3^+ and $C_2H_2^+$ indicate that the major chemical channel for the production of $C_2H_3^+$ in the hollow cathode is the production of H_3^+ through the electron impact ionization of H_2 and the ion–neutral reaction[84]

$$H_2 + H_2^+ \rightarrow H_3^+ + H \quad (1)$$

followed by the proton hop reaction

$$C_2H_2 + H_3^+ \rightarrow C_2H_3^+ + H_2 \quad (2)$$

We will use the well-known reaction rate constants $k_1 = 2.00 \times 10^{-9}$ cm^3 s^{-1} for (1)[85,86] and $k_2 = 2.90 \times 10^{-9}$ cm^3 s^{-1} for (2).[87] In addition to these main chemical reactions, we also include the following ion–neutral reactions involving $C_2H_2^+$ and $C_2H_3^+$:

$$C_2H_2^+ + H_2 \rightarrow C_2H_3^+ + H \quad (3)$$

$$C_2H_2^+ + C_2H_2 \rightarrow \text{products} \quad (4)$$

$$C_2H_3^+ + C_2H_2 \rightarrow \text{products} \quad (5)$$

$C_2H_3^+$ does not react with H_2.[83] The hydrogen abstraction reaction (3) is very nearly thermoneutral, and its rate constant depends on temperature in a subtle manner.[28,88] Here we simply use the rate constant $k_3 = 1.00 \times 10^{-11}$ cm^3 s^{-1} reported by Smith and Adams.[89] Reactions 4 and 5 leading to $C_4H_x^+$ are polymerization reactions that cause soot formation. We use $k_4 = 1.41 \times 10^{-9}$ cm^3 s^{-1} for (4).[90] A wide range of rate constants have been reported for (5), but we adopt $k_5 = 7.20 \times 10^{-10}$ cm^3 s^{-1}, reported by Anicich *et al.*,[91] for consistency.

TABLE 5: Reaction Rate Constants Used in the Calculations of Section 5 (in cm^3 s^{-1})

$k_r = 1.8 \times 10^{-7}$	$k'_{i2} = 2.5 \times 10^{-9}$
$k'_r = 2.7 \times 10^{-7}$	$k_1 = 2.0 \times 10^{-9}$
$k''_r = 4.5 \times 10^{-7}$	$k_2 = 2.9 \times 10^{-9}$
$k_{i1} = 2.8 \times 10^{-8}$	$k_3 = 1.0 \times 10^{-11}$
$k_{i2} = 3.1 \times 10^{-10}$	$k_4 = 1.4 \times 10^{-9}$
$k'_{i1} = 1.5 \times 10^{-7}$	$k_5 = 7.2 \times 10^{-10}$

Using the results of sections A and B and eqs 1–5 and assuming a steady state during the time when the hollow cathode conducts, we have the following simultaneous equations for the concentrations of ions and neutrals in our hollow cathode discharge.

$$d[H_3^+]/dt = (k_{i1}n_{e1} + k_{i2}n_{e2})[H_2] - (k_2[C_2H_2] + k_r n_e)[H_3^+] = 0 \quad (6)$$

$$d[C_2H_2^+]dt = (k'_{i1}n_{e1} + k'_{i2}n_{e2})[C_2H_2] - (k_3[H_2] + k_4[C_2H_2] + k'_r n_e)[C_2H_2^+] = 0 \quad (7)$$

$$d[C_2H_3^+]/dt = k_2[C_2H_2][H_3^+] + k_3[C_2H_2^+][H_2] - (k_5[C_2H_2] + k''_r n_e)[C_2H_3^+] = 0 \quad (8)$$

In eq 6 the production rate of H_3^+ is equated to the ionization rate of H_2 because the ensuing ion–neutral reaction (1) is much faster than the initial step. The k_{i1} and k_{i2} of eqs 6 and 7 represent ionization rate constants due to primary and secondary electrons, respectively. The depletion rate of cations to the cathode is neglected in view of the small electric field in the central part of the hollow cathode probed by the multipassed infrared beam. The numerical values of the rate constants in eqs 6–8 have been discussed earlier and are summarized in Table 5.

Equations 6–8 yield the following formulas for the ion concentrations.

$$[H_3^+] = \frac{(k_{i1}n_{e1} + k_{i2}n_{e2})}{k_2[C_2H_2] + k_r n_e}[H_2] \quad (9)$$

$$[C_2H_2^+] = \frac{(k'_{i1}n_{e1} + k'_{i2}n_{e2})}{k_3[H_2] + k_4[C_2H_2] + k'_r n_e}[C_2H_2] \quad (10)$$

$$[C_2H_3^+] = \frac{k_2[C_2H_2][H_3^+] + k_3[C_2H_2^+][H_2]}{k_5[C_2H_2] + k''_r n_e} \quad (11)$$

In the numerical calculation we use $[H_2] = 3.9 \times 10^{16}$ cm^{-3} and $[C_2H_2] = 1.1 \times 10^{15}$ cm^{-3} corresponding to the pressure used in the experiment and assuming a temperature of 0 °C. The most uncertain quantities are the concentrations of the primary, secondary, and ultimate electrons n_{e1}, n_{e2}, and n_e. We assume these numbers such that they approximately meet the following conditions.

(1) Previous diagnostic study of the negative glow showed a decrease by approximately 2 orders of magnitude in the series n_e, n_{e2}, n_{e1}.[56]

(2) The concentration of $C_2H_3^+$ estimated from the intensities of the observed lines is $\sim 3 \times 10^{10}$ cm^{-3}.

(3) n_e must approximately equal the sum of $[C_2H_3^+]$, $[H_3^+]$, and $[C_2H_2^+]$ to maintain neutrality.

On the basis of these constraints, we obtain the following set of values for the concentrations of charged species:

$$n_e = 4 \times 10^{10}\ \mathrm{cm}^{-3} \qquad [C_2H_3^+] = 2.9 \times 10^{10}$$

$$n_{e1} = 1 \times 10^{7}\ \mathrm{cm}^{-3} \qquad [H_3^+] = 0.7 \times 10^{10}$$

$$n_{e2} = 1 \times 10^{9}\ \mathrm{cm}^{-3} \qquad [C_2H_2^+] = 0.2 \times 10^{10}$$

While they are by no means accurate solutions of the rate equations, we believe that they reflect correct orders of magnitude of charge concentrations in the hollow cathode discharge. The value of n_e is constrained by the conditions (2) and (3) and the values of n_{e1} and n_{e2} by (1). The value of n_e also agrees approximately with the estimate from the current density and the electron mobility in the plasma.[54] The concentration $\sim 10^9$ cm^{-3} of hot electrons is in agreement with the results of diagnostic studies of the negative glow,[56,58,62] while that of ultimate electrons, 4×10^{10} cm^{-3}, is smaller by 1 order of magnitude than what has generally been found previously in He plasmas. This is probably explained as due to the small recombination cross section of He^+ compared with those of molecular ions and to the small concentration of He_2^+ in the He discharges used for the diagnostic studies. The result of Franck and Schlosser[58] using H_2 discharges seems to be more in line with the present result.

The ion concentrations $[C_2H_3^+]$, $[H_3^+]$, and $[C_2H_2^+]$ agree approximately with the estimate from their observed spectral intensities, although the value of $[C_2H_2^+]$ is perhaps too large by a factor of 2. Compared with Amano's estimate of the H_3^+ concentrations in his hollow cathode,[69,70] our overall cation concentration is smaller by 1 order of magnitude. This is because of the presence of C_2H_2, which destroys cations through reactions 2, 4, and 5. In the pure H_2 discharge cations are destroyed by dissociative recombination.[69,70]

D. Summary. The semiquantitative calculations and discussion in this section on the plasma chemistry in our hollow cathode discharge are summarized in the following.

(1) The primary and secondary electrons (hot electrons) ionize H_2 and C_2H_2, and the ultimate electrons at low temperature dissociate cations $C_2H_3^+$, H_3^+, and $C_2H_2^+$ by recombination.

(2) The ionization rate of C_2H_2 is larger than that of H_2 by a factor of 5−7, and the rates due to primary and secondary electrons are comparable.

(3) The main production channel for $C_2H_3^+$ is the production of H_3^+ by eq 1 and the proton hop reaction to C_2H_2 by eq 2. The production of $C_2H_3^+$ by eq 3 is negligible ($\sim$1/30).

(4) The main destruction channel for the cations $C_2H_3^+$, H_3^+, and $C_2H_2^+$ is the reaction with C_2H_2, which is faster than the electron recombination reactions by a factor of 40−440.

(5) Carbocations containing one carbon atom such as CH_2^+ and CH_3^+ are not produced effectively because the rate for dissociative ionization of C_2H_2 breaking the C≡C bond is much smaller ($\lesssim$1/100) than the simple ionization rate.

Acknowledgment. This paper is dedicated to the 60th birthday of Dr. Zdenek Herman. One of the authors (T.O.) has learned much from discussions with him on the physics of ion−neutral reactions. We would like to thank J. E. Lawler for providing useful information on hollow cathode discharges. This research has been supported by NSF Grants PHY-90-22647 and PHY-93-21913.

References and Notes

(1) Oka, T. *Philos. Trans. R. Soc. London A* **1988**, *324*, 81.
(2) Pine, A. S. *J. Opt. Soc. Am.* **1974**, *64*, 1683.
(3) Gudeman, C. S.; Begemann, M. M.; Pfaff, J.; Saykally, R. J. *Phys. Rev. Lett.* **1983**, *50*, 727.
(4) Rösslein, M.; Gabrys, C. M.; Jagod, M.-F.; Oka, T. *J. Mol. Spectrosc.* **1992**, *153*, 738.
(5) Crofton, M. W.; Kreiner, W. A.; Jagod, M.-F.; Rehfuss, B. D.; Oka, T. *J. Chem. Phys.* **1985**, *83*, 3702.
(6) Crofton, M. W.; Jagod, M.-F.; Rehfuss, B. D.; Kreiner, W. A.; Oka, T. *J. Chem. Phys.* **1988**, *88*, 666.
(7) Jagod, M.-F.; Gabrys, C. M.; Rösslein, M.; Uy, D.; Oka, T. *Can. J. Phys.* **1994**, *72*, 1192.
(8) Crofton, M. W.; Jagod, M.-F.; Rehfuss, B. D.; Oka, T. *J. Chem. Phys.* **1987**, *86*, 3755.
(9) Jagod, M.-F.; Rösslein, M.; Gabrys, C. M.; Rehfuss, B. D.; Scappini, F.; Crofton, M. W.; Oka, T. *J. Chem. Phys.* **1992**, *97*, 7111.
(10) Crofton, M. W.; Jagod, M.-F.; Rehfuss, B. D.; Oka, T. *J. Chem. Phys.* **1989**, *91*, 5139.
(11) Rösslein, M.; Jagod, M.-F.; Gabrys, C. M.; Oka, T. *Astrophys. J.* **1991**, *382*, L51.
(12) Jagod, M.-F.; Rösslein, M.; Gabrys, C. M.; Oka, T. *J. Mol. Spectrosc.* **1992**, *153*, 666.
(13) Schreiner, P. R.; Kim, S.-J.; Schaefer, H. F., III; Schleyer, P. v. R. *J. Chem. Phys.* **1993**, *99*, 3716.
(14) Amano, T. *Philos. Trans. R. Soc. London A* **1988**, *324*, 163.
(15) Amano, T.; Tanaka, K. *J. Chem. Phys.* **1985**, *82*, 1045; **1985**, *83*, 3721.
(16) Amano, T. *Chem. Phys. Lett.* **1986**, *127*, 101; **1986**, *130*, 154.
(17) Nakanaga, T.; Amano, T. *Chem. Phys. Lett.* **1987**, *134*, 195.
(18) Nakanaga, T.; Amano, T. *Mol. Phys.* **1987**, *61*, 313.
(19) Lee, S. K.; Amano, T. *Astrophys. J.* **1987**, *323*, L145.
(20) Amano, T. *Astrophys. J.* **1988**, *330*, L137.
(21) Amano, T.; Warner, H. E. *Astrophys. J.* **1989**, *342*, L99.
(22) Warner, H. E.; Amano, T. *J. Mol. Spectrosc.* **1991**, *145*, 66.
(23) Liang, C.; Hamilton, T. P.; Schaefer, H. F., III *J. Chem. Phys.* **1990**, *92*, 3653.
(24) Klopper, W.; Kutzelnigg, W. *J. Phys. Chem.* **1990**, *94*, 5625.
(25) Lindh, R.; Rice, J. E.; Lee, T. J. *J. Chem. Phys.* **1991**, *94*, 8008.
(26) Bogey, M.; Cordonnier, M.; Demuynck, C.; Destombes, J. L. *Astrophys. J.* **1992**, *399*, L103.
(27) Oka, T.; Morino, Y. *J. Mol. Spectrosc.* **1961**, *6*, 472.
(28) Glassgold, A. E.; Omont, A.; Guélin, M. *Astrophys. J.* **1992**, *396*, 115.
(29) Bogey, M.; Bolvin, H.; Cordonnier, M.; Demuynck, C.; Destombes, J. L.; Escribano, R.; Gomez, P. C. *Can. J. Phys.* **1994**, *72*, 967.
(30) Escribano, R. S.; Bunker, P. R.; Gomez, P. C. *Chem. Phys. Lett.* **1988**, *150*, 60.
(31) Vager, Z.; Zajfman, D.; Graber, T.; Kanter, E. P. *Phys. Rev. Lett.* **1993**, *71*, 4319.
(32) Kanter, E. P.; Vager, Z.; Both, G.; Zajfman, D. *J. Chem. Phys.* **1986**, *85*, 7487.
(33) Pine, A. S. *J. Opt. Soc. Am.* **1976**, *66*, 97.
(34) Pursell, C. J.; Weliky, D. P.; Ho, W. C.; Takagi, K.; Oka, T. *J. Chem. Phys.* **1989**, *91*, 7997.
(35) Ho, W. C.; Pursell, C. J.; Weliky, D. P.; Takagi, K.; Oka, T. *J. Chem. Phys.* **1990**, *93*, 87.
(36) Pursell, C. J.; Weliky, D. P.; Oka, T. *J. Chem. Phys.* **1990**, *93*, 7041.
(37) van den Heuvel, F. C.; Dymanus, A. *Chem. Phys. Lett.* **1982**, *92*, 219.
(38) Foster, S. C.; McKellar, A. R. W.; Sears, T. J. *J. Chem. Phys.* **1984**, *81*, 578.
(39) Watson, J. K. G. In *Vibrational Spectra and Structure*; Durig, J. R., Ed.; Elsevier: New York, 1977; Vol. 6, pp 1−89.
(40) Raine, G. P.; Schaefer, H. F., III *J. Chem. Phys.* **1984**, *81*, 4034. Lee, T. J.; Schaefer, H. F., III *J. Chem. Phys.* **1986**, *85*, 3437.
(41) Paschen, F. *Ann. Phys. (Leipzig)* **1916**, *50*, 901.
(42) Tolansky, S. *High Resolution Spectroscopy*; Methuen and Co.: London, 1947.
(43) Schüler, H. *Phys. Z.* **1921**, *22*, 264.
(44) Schüler, H. *Z. Phys.* **1926**, *37*, 868.
(45) Schüler, H. *Z. Phys.* **1926**, *35*, 323; **1930**, *59*, 149.
(46) Francis, G. In *Encyclopedia of Physics*, Vol. XXII, *Gas Discharges II*; Flüngge, S., Ed.; Springer-Verlag: Berlin, 1956; pp 53−208.
(47) Herzberg, G. *J. Chem. Phys.* **1979**, *70*, 4806.
(48) Dabrowski, I.; Herzberg, G. *Can. J. Phys.* **1980**, *58*, 1238.
(49) Herzberg, G.; Watson, J. K. G. *Can. J. Phys.* **1980**, *58*, 1250.
(50) Herzberg, G.; Lew, H.; Sloan, J. J.; Watson, J. K. G. *Can. J. Phys.* **1981**, *59*, 428.
(51) Majewski, W. A.; Marshall, M. D.; McKellar, A. R. W.; Johns, J. W. C.; Watson, J. K. G. *J. Mol. Spectrosc.* **1987**, *122*, 341.
(52) Majewski, W. A.; Feldman, P. A.; Watson, J. K. G.; Miller, S.; Tennyson, J. *Astrophys. J.* **1989**, *347*, L51.
(53) Paschen, F.; Ritschl, R. *Ann. Phys. (Leipzig)* **1933**, *18*, 867.
(54) von Engel, A. *Ionized Gases*; Oxford University Press: London, 1965; reprinted AIP Press: Woodbury, NY, 1993.

(55) von Engel, A. *Electric Plasmas: Their Nature and Uses*; Taylor and Francis: New York, 1983.
(56) Pringle, D. H.; Farvis, W. E. *Phys. Rev.* **1954**, *96*, 536.
(57) Anderson, J. M. *J. Appl. Phys.* **1960**, *31*, 511.
(58) Franck, G.; Schlosser, E. *Z. Phys.* **1969**, *224*, 222.
(59) Heisen, A.; Wunderer, B. *Z. Phys.* **1969**, *224*, 237.
(60) Emeleus, K. G. *J. Phys. D* **1981**, *14*, 2179.
(61) Den Hartog, E. A.; O'Brian, T. R.; Lawler, J. E. *Phys. Rev. Lett.* **1989**, *62*, 1500.
(62) Lawler, J. E.; Den Hartog, E. A.; Hitchon, W. N. G. *Phys. Rev. A* **1991**, *43*, 4427.
(63) Langmuir, I. *Phys. Rev.* **1925**, *26*, 585.
(64) Mitchel, J. B. A. *Phys. Rep.* **1990**, *186*, 215.
(65) Dalgarno, A. *Adv. Atom. Mol. Phys.* **1994**, *32*, 57.
(66) Leu, M. T.; Biondi, M. A.; Johnsen, R. *Phys. Rev. A* **1973**, *8*, 413.
(67) Adams, N. G.; Smith, D. In *Astrochemistry IAU Symposium 120*; Vardya, M. S., Tarafdar, S. P., Eds.; Reidel: Dordrecht, 1987; p 1.
(68) Adams, N. G.; Smith, D. In *Dissociative Recombination: Theory, Experiment, and Applications*; Mitchell, J. B. A., Guberman, S. L., Eds.; World Scientific: Singapore, 1989; p 124.
(69) Amano, T. *Astrophys. J.* **1988**, *329*, L121.
(70) Amano, T. *J. Chem. Phys.* **1990**, *92*, 6492.
(71) Canosa, A.; Gomet, J. C.; Rowe, B. R.; Mitchell, J. B. A.; Queffelec, J. L. *J. Chem. Phys.* **1992**, *97*, 1028.
(72) Larsson, M.; Danared, H.; Mowat, J. R.; Sigray, P.; Sundström, G.; Broström, L.; Filevich, A.; Källberg, A.; Mannervik, S.; Rensfelt, K. G.; Datz, S. *Phys. Rev. Lett.* **1993**, *70*, 430.
(73) Yousif, F. B.; van der Donk, P.; Mitchell, J. B. A. *J. Phys. B* **1993**, *26*, 4249.
(74) Sundström, G.; Mowat, J. R.; Danared, H.; Datz, S.; Broström, L.; Filevich, A.; Källberg, A.; Mannervik, S.; Rensfelt, K. G.; Sigray, P.; Ugglas, M.; Larsson, M. *Science* **1994**, *263*, 785.
(75) Smith, D.; Spanel, P. *Int. J. Mass Spectrom. Ion Processes* **1993**, *129*, 163.
(76) Smith, D.; Spanel, P. *Chem. Phys. Lett.* **1993**, *211*, 454.
(77) Fehér, M.; Rohrbacher, A.; Maier, J. P. *Chem. Phys.* **1994**, *185*, 357.
(78) Mul, P. M.; McGowan, J. W. *Astrophys. J.* **1980**, *237*, 749.
(79) Kieffer, J. L. *At. Data* **1969**, *1*, 19.
(80) Rapp, D.; Englander-Golden, P. *J. Chem. Phys.* **1965**, *43*, 1464.
(81) Tate, J. T.; Smith, P. T. *Phys. Rev.* **1932**, *39*, 270.
(82) Gaudin, A.; Hagemann, R. *J. Chim. Phys.* **1967**, *64*, 1209.
(83) Anicich, V. G.; Huntress, W. T., Jr. *Astrophys. J. Suppl. Ser.* **1986**, *62*, 553.
(84) Oka, T. *Rev. Mod. Phys.* **1992**, *64*, 1141.
(85) Clow, R. P.; Futrell, J. H. *Int. J. Mass Spectrom. Ion Phys.* **1972**, *8*, 119.
(86) Theard, L. P.; Huntress, W. T., Jr. *J. Chem. Phys.* **1974**, *60*, 2840.
(87) Mackay, G. I.; Tanaka, K.; Bohme, D. K. *Int. J. Mass Spectrom. Ion Phys.* **1977**, *24*, 125.
(88) Herbst, E.; Yamashita, K. *J. Chem. Soc. Faraday Trans.* **1993**, *89*, 2175.
(89) Smith, D.; Adams, N. G. *Chem. Phys. Lett.* **1977**, *47*, 383.
(90) Kim, J. K.; Anicich, V. G.; Huntress, W. T., Jr. *J. Phys. Chem.* **1977**, *81*, 1978.
(91) Anicich, V. G.; Huntress, W. T., Jr.; McEwan, M. J. *J. Phys. Chem.* **1986**, *90*, 2446.

JP951724D